PROJECT REPORT
2001-32
FINAL PROJECT REPORT

sustainable
forest
management
network

réseau
sur la
gestion durable
des forêts

Oxidation of
Pulp Mill Effluents
in an Impinging-Jet
Ozone Bubble Column

Mohamed Gamal El-Din and Daniel W. Smith

Oxidation of Pulp Mill Effluents in an Impinging-Jet Ozone Bubble Column

SFM Network Project: Maximizing Enhanced Ozone Oxidation of Pulp Mill Effluents

by

Mohamed Gamal El-Din and Daniel W. Smith

Department of Civil and Environmental Engineering
University of Alberta, Edmonton, Alberta

September 2001

EXECUTIVE SUMMARY

Kraft pulp mill effluents may contain high concentrations of color, COD (chemical oxygen demand), and TOC (total organic carbon). Kraft pulp mill effluents also contain detectable concentrations of AOX (halogenated organic halides). Recently, the color and AOX-causing compounds have attracted large attention due to their high resistance to the conventional biological treatment processes. Therefore, the interest has shifted to other treatment alternatives in order to comply with the more stringent effluent discharge regulations. Among those treatment alternatives, ozonation has been recognized as one of the highly promising technologies for treating pulp mill effluents due to rapid reaction rates leading to the reduction of color and AOX-causing compounds.

The scope of this research was to study and evaluate the ozone treatment process in a new design of ozone bubble columns. An impinging-jet bubble column, that utilized two venturi injectors, has been tested for the ozone mass transfer applications in pulp mill wastewater treatment. The venturi injectors were utilized to create turbulent gas-liquid jets in the ambient fluid by placing them at an intersecting angle of 125° and a 60 mm distance between the centers of the nozzles. The intersecting of the gas-liquid jets caused an increase in the turbulence produced in the ambient fluid and therefore, greatly increased the gas-liquid mass transfer.

Using the venturi injectors for sparging the ozone gas into the liquid phase in the impinging-jet contactor has led to a significant increase in the enhanced overall mass transfer coefficient ($Ek_{L}a$) and the enhanced factor (E), compared to other designs of ozone contactors. As a result, the off-gas ozone concentrations that were produced from the impinging-jet contactor were substantially lower than those produced from the other contactors that were operated in a semibatch-flow mode. The ozonation process induced higher reductions in the color and AOX concentrations compared to COD and TOC of the treated Kraft pulp mill effluents. The small ratio of the BOD_5/COD of the treated wastewater indicates the need for further treatment of this type of wastewater to increase its biodegradability, and consequently, to remove the increase in the BOD_5 of the wastewater as a result of applying further treatment. The reduction efficiencies of color, AOX, COD, and TOC indicated that the scale-up and reactor configuration have exhibited insignificant effects on the ozonation treatment levels achieved in the different types of the ozone contactors examined in this study. This suggests that a small scale-up factor was associated with the ozonation treatment of pulp mill effluents.

A 2-D laser particle dynamics analyzer was used to simultaneously measure the bubble size, bubble rise velocity, bubble size distribution, and turbulence intensities in the impinging-jet bubble column. These measurements were conducted in clean deionized water and in a Kraft pulp mill effluent that was ozonated using a wide range of utilized ozone doses. The purpose of ozonation was to investigate the effects on surface tension by changing the pulp mill effluent characteristics, and consequently, on the bubble size, the gas hold-up (ε_G), and the specific gas bubbles' interfacial area (a).

The intersecting of the gas-liquid jets caused an increase in the turbulence produced in the ambient fluid and as a result, the count mean bubble diameter (d_B) and the Sauter mean bubble diameter (d_S) were smaller than those obtained in conventional bubble columns. This has led to a significant increase in the specific gas bubbles' interfacial area compared to that in conventional bubble columns. The count mean bubble and Sauter mean bubble diameters were found to be dependent on the superficial gas and liquid velocities (u_G and u_L, respectively). As u_L increased, d_S decreased slightly. During the aeration of the deionized water, an increase in u_G caused a slight decrease in d_B. Meanwhile, as u_G increased during the aeration of the raw Kraft pulp mill effluent, d_B increased slightly then it started decreasing. During the aeration of the preozonated Kraft pulp mill effluent, an increase in u_G caused d_B to decrease. The count and Sauter mean bubble diameters were smaller in the raw Kraft pulp mill effluent compared to those in the deionized water. This has led to a significant increase in the specific bubble interfacial area and gas hold-up compared to those in the deionized water. As the raw Kraft pulp mill effluent was ozonated and the amount of utilized ozone increased, the count mean and Sauter mean bubble diameters increased. A possible explanation for that could be due to changes in the surface tension characteristics as a result of partial or complete oxidation and/or destruction of the polar organic compounds, and the inorganic compounds present in the raw Kraft pulp mill effluent. The bubble size distributions exhibited different trends depending on the type of the test liquid and on the operating conditions in terms of u_G and u_L. Generally, those distributions could be well described using normal, gamma, or log-normal density functions.

ACKNOWLEDGEMENTS

INTRODUCTION

Kraft pulp mill effluents may contain high concentrations of color, COD (chemical oxygen demand), and TOC (total organic carbon). Kraft pulp mill effluents also contain detectable concentrations of AOX (halogenated organic halides). Recently, the color and AOX-causing compounds have attracted large attention due to their high resistance to the conventional biological treatment processes. Therefore, the interest has shifted to other treatment alternatives in order to comply with the more stringent effluent discharge regulations (Haberl et al. 1991; Zhou and Smith 1997). Among those treatment alternatives, ozonation has been recognized as one of the highly promising technologies for treating pulp mill effluents due to its high induced reduction efficiencies of color and AOX-causing compounds (Bauman and Lutz 1974; Nebel et al. 1974; Zhou and Smith 2000a).

Through fast oxidation reactions, ozone can selectively react with the color-causing (chromophoric) and AOX-causing (halogenated) functional groups as a result of the their electrophilic nature (Bauman and Lutz 1974; Nebel et al. 1974). The color reduction efficiency was found to be dependent mainly on the amount of the utilized ozone (ΔO_3) and to some extent on the wastewater initial characteristics in terms of color, COD, pH and dissolved and suspended solids. Zhou and Smith (1997, 2000) investigated the ozonation effects on reducing color and AOX-causing compounds from a biologically treated Kraft pulp mill wastewater. In the semibatch experiments, maximum reduction efficiencies up to 75 % and 50 % of the color and AOX-causing compounds, respectively, were achieved at a utilized ozone dose of 125 mgL^{-1}. In their pilot-scale experiments, the maximum reduction efficiencies were up to 60 % and 30 % of the color and AOX-causing compounds, respectively, at a utilized ozone dose up to 125 mgL^{-1}. As the utilized ozone dose increased to 240 mgL^{-1}, the reduction efficiencies of color and AOX-causing compounds increased up to 80 % and 45 %, respectively. The pulp mill wastewater biodegradability can be improved as a result of the conversion of the high-molecular-weight organic compounds to low-molecular-weight organic compounds through the ozone oxidation reactions (Zhou and Smith 1997). Zhou and Smith (1997) reported that he pulp mill effluent BOD$_5$ increased by about 165 % at a utilized ozone dose of 175 mgL^{-1}. Applying a hybrid ozonation-biological treatment process can help achieving higher treatment levels (Zhou and Smith 1997; Heinzel et al. 1992). In general, the ozonation treatment induced low reduction efficiencies of the COD and TOC-causing compounds as observed in several studies (Zhou and Smith 1997; Mohammed and Smith 1992). The modeling of the induced reduction of color, AOX, TOC, and COD, caused by the ozonation process, can lead to more understanding of the effects of the various operating parameters on the performance of the ozonation process. Quantifying the ozonation process parameters and the process treatment efficiencies in various designs of ozonation systems and over a wide range of operating conditions will lead to a reliable and accurate scale-up of the ozonation process.

The ozonation experimental results obtained in three different types of ozone contactors were analyzed to investigate the effects of the ozone contactor design, configuration, operating conditions, and scale-up on the ozonation process reduction efficiencies of the impurities found

in Kraft pulp mill effluents and the increase in the biodegradability of this type of wastewater. The three types of ozone contactors included: (1) an extra-coarse-bubble diffuser ozone contactor; (2) an impinging-jet ozone contactor; and (3) a fine-bubble diffuser ozone contactor.

Gas hold-up (ε_G) is one of the important variables that characterize the hydrodynamics of the gas-liquid, i.e., the two-phase flows, in bubble columns. It is defined as the fraction of the dispersed volume occupied by the gas bubbles. ε_G can affect the performance of bubble columns in two ways: (1) it provides the fractional volume of the gas phase and therefore, its residence time inside the reactor; and (2) in conjunction with the knowledge of the Sauter mean (i.e., volume-to-surface area mean) bubble diameter, it allows the determination of the specific bubble interfacial area (Jamialahmadi and Müller-Steinhagen 1992). Gas hold-up, Sauter mean diameter, and specific gas bubbles' interfacial area are interrelated through the following relationship:

$$a = \frac{A}{V} = \frac{6\varepsilon_G}{d_S} \qquad [1]$$

where: a = mean specific gas bubbles' interfacial area (m^{-1}), A = mean gas bubbles' surface area (m^2), V = volume of the dispersed phases (m^{-3}), ε_G = gas hold-up ($m^3 m^{-3}$), and d_S = Sauter mean bubble diameter (m). Since the overall mass transfer coefficient ($k_L a$) can be measured experimentally and with the knowledge of a, the local mass transfer coefficient (k_L) can be determined for the gas-liquid flow in bubble columns.

The use of computational fluid dynamics (CFD) has grown over the past decade since it can offer detailed predictions of the behaviour and the characteristics of multiphase flows such as gas-liquid flow in bubble columns. CFD can lead to significant improvements in the area of scale-up of bubble columns. In order to achieve successful application of CFD in the scale-up process, a better understanding of the fundamentals of the gas-liquid flow phenomena has to be provided. Gas-liquid flows are complex in their nature and their behaviour can vary substantially depending on the design, configuration, and operating conditions of the bubble columns. It is very hard to conduct experimental measurements inside gas-liquid flows because of their sensitive nature to any disturbances caused by intrusive measuring devices such as electric probes (Mudde et al. 1998). As a result, the use of non-intrusive measurement techniques such as laser Doppler anemometry (LDA) and Phase Doppler anemometry (PDA) can provide great tools for characterization and better understanding of the local rather than the global flow phenomena in gas-liquid flows (Mudde et al. 1998).

Several studies have been conducted for measuring the size of gas bubbles in air-water systems by using a photographic technique (Akita and Yoshida 1974; Yamashita et al. 1978; Roustan et al. 1996). They observed that, especially at higher gas throughputs, the bubbles were not spherical but could be approximated by oblate ellipsoids. Yamashita et al. (1978) measured the d_S of the ellipsoidal bubbles using a photographic study. Alternatively, and assuming that the bubbles are perfect spheres, they measured the d_S of the bubbles using an electric probe. Interestingly, and at low gas throughputs, they observed that the two measures of the mean d_S

were almost identical. Also, from their photographic measurements, they observed that d_B was almost equal to d_S.

In the current study, a 2-D laser particle dynamics analyzer, that utilizes phase Doppler anemometry (PDA) and laser Doppler anemometry (LDA), was used to obtain simultaneous measurements of: (1) the bubble size; (2) the bubble size distributions; (3) the gas-phase axial and radial velocity distributions; and (4) the gas-phase turbulence intensities in the axial and radial directions in the impinging-jet bubble column. Two types of liquids were tested: clean deionized water and Kraft pulp mill effluent. The Kraft pulp mill effluent was ozonated using a wide range of utilized ozone doses to investigate its effects on pulp mill effluent characteristics. Of primary interest was its surface active agents (SAA) content and the resulting effect on the surface tension and consequently, on the bubble size (d_B and d_S), the gas hold-up (ε_G), and the specific gas bubbles' interfacial area (a). The gas and liquid flowrates were varied in order to determine their effects on the bubble size, the specific bubble interfacial area, and the gas hold-up.

DATA ANALYSIS

Ozonation Tests: Experimental Methods
Extra-coarse-bubble diffuser ozone contactor
The ozonation tests were conducted in a semibatch-flow mode in an extra-coarse-bubble diffuser contactor. A detailed schematic of the experimental set-up is shown in Figure 1. The ozone contactor was made from PVC with an inside diameter of 570 mm and a total height of 900 mm. The headspace was restricted to only 6 % of the total reactor volume to shorten the lag-time for the ozone off-gas to travel through the exhaust-gas line to the off-gas ozone monitor. An average volume of 2.1×10^{-1} m^3 of a Kraft pulp mill effluent was pumped into the reactor. Ozone gas was generated from extra-dry pure oxygen as the feed gas using a corona discharge ozone generator (model GLS-7, PCI-WEDECO®). The ozone generator was allowed to stabilize for about 1,800 s in order to obtain a stable ozone concentration in the feed gas. The feed gas, that contained an ozone concentration in the range from 4.0 to 8.1 % w/w, was sparged into the liquid phase through a set of eight extra-coarse diffusers (95 mm x 15 mm) that were equally spaced over the cross-sectional area of the contactor and elevated about 10 mm from the bottom of the contactor to provide better contact between the gas bubbles and the liquid phase. The feed-gas flowrate ranged from 2.7×10^{-4} to 3.2×10^{-4} m^3s^{-1}. Those flowrates corresponded to superficial gas velocities ranging from 1.0×10^{-3} to 1.2×10^{-3} ms^{-1}. In order to achieve different utilized ozone doses of up to 230 mgL^{-1}, the ozonation time was varied up to 2,820 s. During the ozonation tests, the ozone concentrations in the feed-gas and off-gas were continuously monitored using PCI-WEDECO® ozone monitors (models HC400 and LC, respectively). Those monitors were allowed at least 900 s to stabilize before registering their readings. Periodic calibration of the ozone monitors was conducted using the KI method as described by the Standard Methods for Examination of Water and Wastewater (APHA-AWWA-WEF, 1995). All the materials that came in contact with the dissolved and gaseous ozone during the experiments

were made of glass, teflon, stainless steel, or PVC to reduce the possible interference that would result from the reactions between ozone and the experimental set-up components.
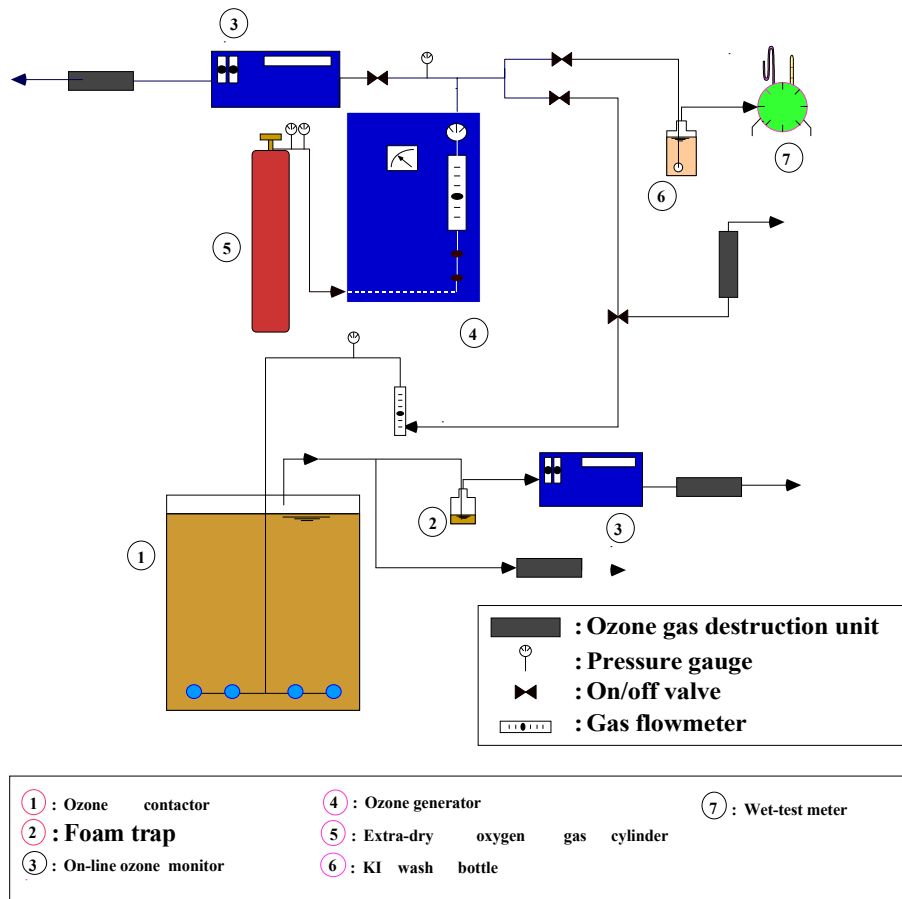

Figure 1.   Schematic of the experimental set-up of the extra-coarse-bubble diffuser ozone contactor.

Impinging-jet ozone contactor

Continuous-flow mode

The ozonation experiments were conducted in a pilot-scale impinging-jet bubble column (see Figure 2) in a continuous-flow mode. The bubble column was made from PVC and had an inside diameter of 100 mm and a total height of 1520 mm. The water depth was kept constant at 1315 mm by placing an overflow weir at the top of the column. A ring tube was also installed at the top of the column with a 20 mm-diameter hole facing downward. The Kynar Mazzei® venturi injectors had an inside diameter of 12.7 mm and were placed 25 mm above the bottom of the column. The injectors were placed at an intersecting angel of 125° and the distance between the centers of the nozzles was 60 mm. The bubble column had an elliptical base to reduce the effect of the backward jet that was created in the ambient fluid as a result of the jet impingement. The sidewalls of the bottom part of the column had a conical shape. With this configuration at the bottom of the column, dead pocketing effects were minimized. Based on the above reactor

4

configuration, it was reasonably assumed that the backmixing along the column height was relatively uniform. The same protocols as described in the previous section, concerning the generation of the ozone gas and the monitoring of the ozone concentrations in the feed and exhaust-gas lines, were applied during the ozonation experiments conducted in the impinging-jet bubble column. Again, all the materials that came in contact with the dissolved and gaseous ozone during the experiments were made of glass, teflon, stainless steel, or PVC. The ozone contactor was operated in a co-current flow mode under two modes of the gas sparging: (1) positive pressure (i.e., injection) mode; and (2) vacuum or negative pressure (i.e., ejection) mode. At least eight turnovers of the reactor working volume were allowed for the ozonation process to reach isothermal steady-state conditions that was verified by reaching a constant off-gas ozone concentration in the exhaust-gas line.
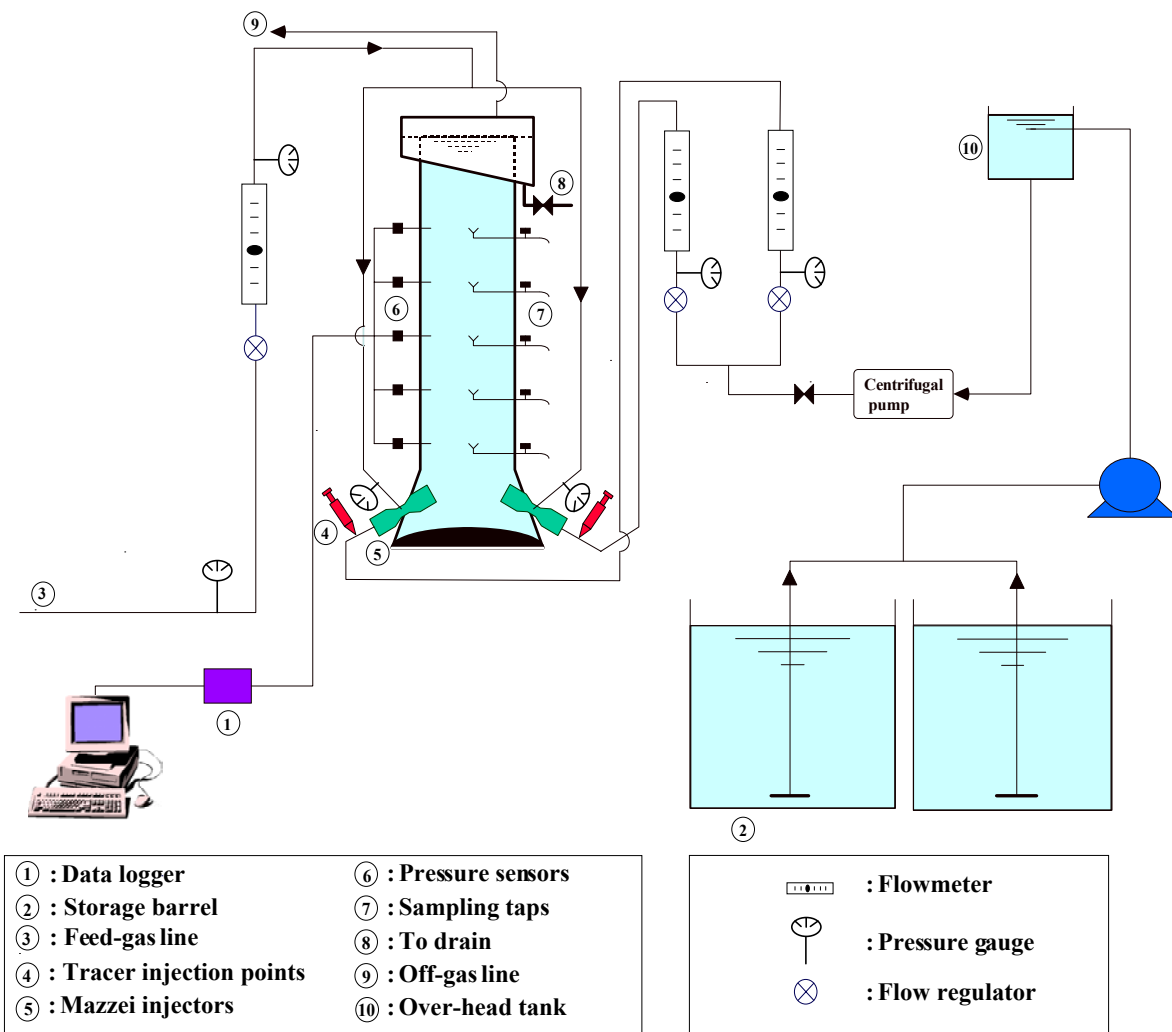

Figure 2.   Schematic of the experimental set-up of the pilot-scale impinging-jet ozone contactor.

The liquid flowrate ranged from 6.2 x 10^{-5} to 2.2 x 10^{-4} $m^3 s^{-1}$ leading to an average theoretical hydraulic retention time in the range of 48 to 174 s. During the ozonation experiments, the feed-

gas flowrate ranged from 1.4 x 10^{-5} to 1.1 x 10^{-4} m^3s^{-1}, the feed-gas ozone concentration ranged from 9.0 to 11.0 % w/w, and the pulp mill effluent temperature ranged from 16.0 to 25.0 ^{o}C. The raw pulp mill effluent characteristics were variable over time and the average characteristics of the pulp mill effluent used in the current study are shown in Table 1.

Semibatch-flow mode

The same operating conditions used in the pulp mill effluent ozonation tests that were operated in the continuous-flow mode, were used in the experiments conducted under semibatch-flow conditions as the liquid-phase was recirculated while the gas-phase was continuously introduced through the injectors' throats. Those experiments were conducted for the purpose of investigating the effects of the ozone contact time (t) and the corresponding amount of the utilized ozone (ΔO_3) on the: (1) ozone gas absorption dynamics in terms of the enhanced overall mass transfer coefficient (Ek_La) and the enhancement factor (E); and (2) the off-gas ozone concentration. Therefore, the ozone contact time was varied from 240 to 2,880 s.

Table 1.　　　　Average characteristics of the raw pulp mill effluent

Wastewater parameters	Average concentrations				
	Extra-coarse-bubble diffuser ozone contactor	Impinging-jet ozone contactor		Fine-bubble diffuser ozone contactor	
	Semibatch-flow mode	Continuous-flow mode	Semibatch-flow mode	Continuous-flow mode	Semibatch-flow mode
Color (TCU)	1129	1199	1106	1213	1223
AOX (mgL^{-1})	9.6	10.1	11.2	9.1	7.8
COD (mgL^{-1})	671	750	681	607	485
TOC (mgL^{-1})	268	250	240	239	192
BOD$_5$ (mgL^{-1})	16.5	21.5	18.8	9.1	11.0
pH	7.7	7.7	7.6	7.6	7.6

Fine-bubble diffuser ozone contactor

Zhou and Smith (1997) conducted bench-scale and pilot-scale ozonation experiments in a fine-bubble diffuser ozone contactor. They investigated the ozonation treatment efficiencies and the ozone gas absorption dynamics in two different scales of the fine-bubble diffuser ozone contactor and under two different modes of operation: (1) the semibatch-flow mode; and (2) the continuous-flow mode. The liquid phase used in their experiments was Kraft pulp mill effluent that was discharged from an aerated lagoon basin of a Kraft pulp mill. Detailed description of the experimental protocols and the experimental set-up can be found in Zhou and Smith (1997). The raw pulp mill effluent characteristics were variable over time and the average characteristics of the pulp mill effluent used in the study of Zhou and Smith (1997) are shown in Table 1.

Characterization of the pulp mill wastewater

Before and after ozonation, samples of the pulp mill wastewater were analyzed to determine the ozonation process induced treatment efficiencies. These analyses were performed to determine the color, AOX, COD, TOC, and BOD_5. The true color was analyzed according to the H5.P method suggested by the Canadian Pulp and Paper Association (1974). AOX was analyzed using Euroglas AOX analyzer according to the adsorption-pyrolysis- titrimetric method (APHA-AWWA-WEF 1995). COD was analyzed according to the closed reflux-colorimetric method (APHA-AWWA-WEF 1995) by employing silver-catalyzed oxidation with potassium dichromate in sulfuric acid. TOC was analyzed according to the combustion-infrared method (APHA-AWWA-WEF 1995) using a Dohrmann carbon analyzer (model DC-80®).

Bubble Characterization Tests: Experimental Methods

Particle dynamics analyzer

Operating principle

The operating principle of the particle dynamics analyzer can be explained through the use of a simple fringe model. An optical system is used to split a continuous laser beam into two parallel beams. As the two beams pass through a spherical lens, they get reflected and consequently they intersect at the focal point of the lens. Two sets of plane parallel interference fringes are produced, at the intersection point of the laser beams, in the Y-Z and X-Z planes. The spacing between the fringes depends on the intersecting angle and the laser wavelength.

Principle of the bubble rise velocity measurement

The laser Doppler anemometry (LDA) is utilized for measuring the velocity of the bubbles in a gas-liquid flow. As the bubbles rise inside the column and pass through the interference fringes, that are formed in an ellipsoidal volume or referred to as the probe or measurement volume, they will cause a scattering of the light in different directions. The scattered light, received by the receiving optics, will have another frequency as a result of the Doppler effect. The Doppler burst is detected by a high-speed photo-multiplier and converted into an electronic signal that will have a frequency proportional to the bubble rise velocity. Therefore, the measurement of those frequencies will allow the determination of the bubble rise velocity. The frequency of the scattered light will carry no information of the sign of the velocity of the bubble. To overcome this velocity sign ambiguity, a small frequency shift is introduced in the transmitting optics to one of the crossing laser beams. As a result, the fringe pattern is no longer stationary but moves perpendicularly to the fringe plane and the light intensity at any point will be modulated at the shift frequency. A bubble moving in the probe volume will scatter light such that the difference between the modulation frequency and the shift frequency is proportional to the velocity. Therefore, for a bubble moving in the opposite direction to the fringe movement, the modulation frequency will increase. Meanwhile, for a bubble moving in the same direction of the fringe movement, the modulation frequency will decrease. In order to achieve that, a 40 MHz frequency shift was applied via the use of a Bragg cell.
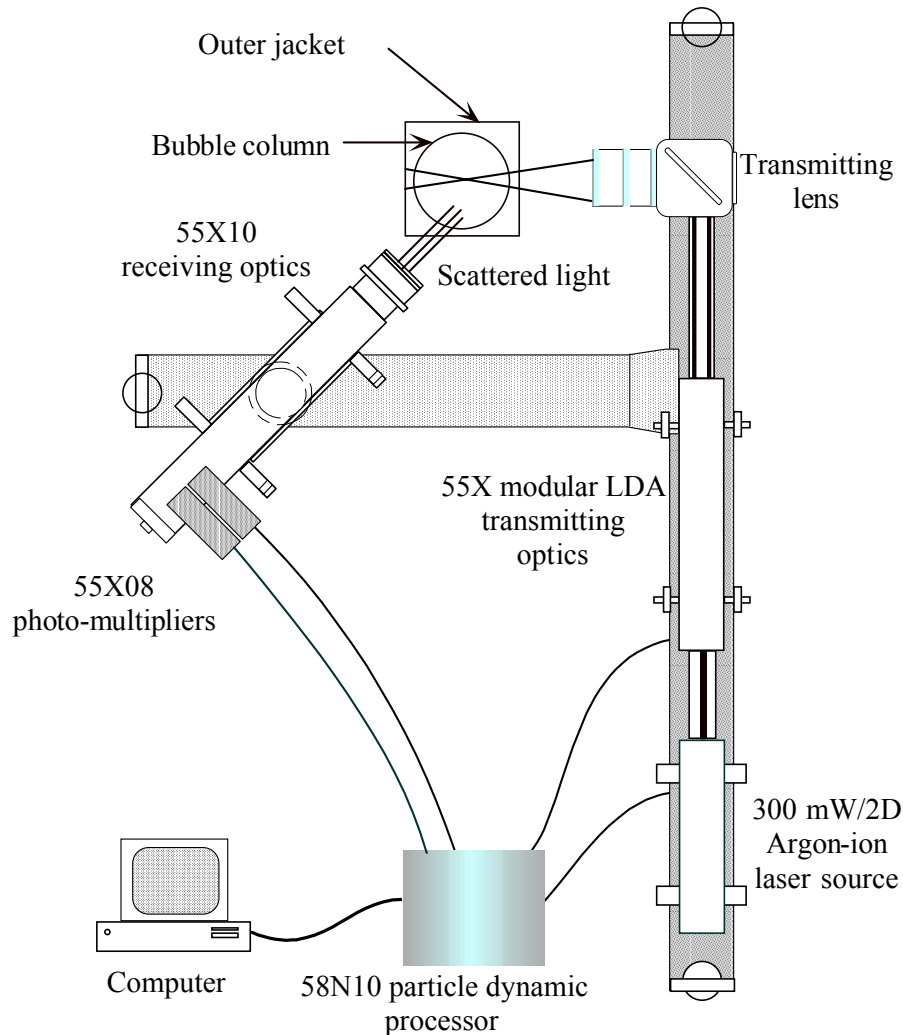
Figure 3.   Components of the particle dynamics analyzer set-up (adapted from Shawwa 1998).

Principle of the bubble size and concentration measurements

The laser Doppler anemometry (LDA) and phase Doppler anemometry (PDA) are utilized for measuring the size and concentration of the bubbles in a gas-liquid flow. As the bubbles pass through the probe volume, they scatter the light. The scattered light will contain information about the bubble size. The PDA operating principle can be explained using a fringe model of the phase shift. Considering the interference fringes in the probe volume to be light rays, they are reflected and refracted by the transparent gas bubbles as they pass through the probe volume. A set of two detectors are located at separate locations and will observe alternately light and dark fringes at the same frequency with a relative phase proportional to the spacing between the detectors divided by the spacing between the projected fringes. The spacing between the projected fringes at the location of the detectors is inversely proportional to the effective focal length of the bubble that is proportional to the bubble diameter (d_B). Therefore, the measured phase shift is proportional to d_B of the bubble passing through the probe volume. In order to obtain an exact and accurate linear relationship between d_B and the phase shift, a

scattering pattern has to be dominant. The refractive index of water is larger than that of air. Therefore, a 70° scattering angle in a forward scattering mode provides the highest signal levels and an excellent linear relationship between the phase shift and the bubble diameter for measuring the size of an air bubble moving in water (DANTEC 1989).

The concentration of the bubbles (C_B) can be determined based on the knowledge of the arrival rate and the velocity of the rising bubble as well as the cross-sectional area of the probe volume. The cross-sectional area of the probe volume is a function of the laser power, the electronic sensitivity, and the size of the bubble passing through the laser beam. For a bubble to be detected, the light level must be above a fixed detection threshold. Large bubbles can pass near the edge of the probe volume and still be detected as a result of their ability to scatter more light than small bubbles. Consequently, the concentrations obtained by the PDA will be biased towards large bubbles. This ambiguity in concentration determination is resolved by using the residence time of the bubble as a weighting factor for the bubble size distribution.

PDA configuration and operational settings adjustment

A 2-D DANTEC$^®$ laser particle dynamics analyzer was used in the current study. It consisted of (1) 55X modular LDA transmitting optics; (2) 57X10 receiving optics; (3) 55X08 photo-multipliers; and (4) 58N10 processor. The set-up of the PDA is shown in Figure 3. The configuration and operational settings used in the current study are presented in Table 2. Those settings were chosen after investigating a wide range of PDA operational configurations and settings to match the velocity and bubble size measurements with those obtained in a photographic study. Therefore, the information obtained from the photographic study helped in adjusting the transmitting and receiving optics configuration and the electronics' operational settings to obtain accurate and reliable results.

Digital photographic measurements of the bubble size and the bubble rise velocity

Measurements of the bubble size and the bubble rise velocity were conducted using a Canon Powershot G1$^®$ digital camera. The same operating conditions and the location of measurements that were to be used during the PDA measurements were applied in the photographic study. The camera was leveled and mounted on a stable tripod. An adequate source of light was used and the lens of the camera was focused on a fixed vertical line at the center of the column before the photographic images were recorded. The video photographic study provided rough estimates of the bubble rise velocity by selecting a swarm of bubbles and recording the time it took them to rise over a certain distance along the column height. The rate of video capture was 15 frames per second and the resolution was adjusted to 320/240 pixels. The video images were downloaded and viewed using digital video software. The shutter speed was adjusted to 1/1000 s during the capture of still digital images and the resolution was adjusted to 2048/1536 pixels. Measurements of the bubble size were conducted by selecting a number of individual bubbles that were sharply focused allowing for the shapes and sizes of the bubbles to be obtained. The size measurements were corrected using the proper scale factor that was obtained by mounting a measuring tape of a known scale in the area where the photographic images were recorded. The photographic study was conducted only for the clean deionized water

due to the difficulties encountered in obtaining high-quality images when Kraft pulp mill was used as the test liquid. This was a result of the high color content of the effluent.

Table 2.   PDA configuration and operational settings

Laser specifications	
Argon-Ion Laser Power (mW)	300
Bragg Cell Frequency Shift (MHz)	40
U-velocity Laser beam wavelength, λ (nm)	514.5
V-velocity Laser beam wavelength, λ (nm)	488.0
Electronics set-up	
Signal bandwidth (MHz)	0.12
Validation level during DI water experiments (dB)	0
Validation level during Kraft pulp mill effluent experiments (dB)	-3
Spherical validation	no
Gain	high
Transmitting optics set-up	
Front lens focal length (mm)	600
Laser beam spacing (mm)	12
Fringe spacing, $\delta_{f,x}$ (μm)	25.726
Fringe spacing, $\delta_{f,y}$ (μm)	24.401
Number of fringes	8
Measurement volume dimensions, δ_x x δ_y x δ_z (mm x mm x mm)	0.2159 x 0.2159 x 28.804
Frequency shift sign	positive
Polarization angle (degree)	0
Polarization orientation w.r.t. scattering plane	parallel
Gaussian beam diameter (mm)	0.82
Beam expansion ratio	1.85
Beam collimation ratio	1.20
Receiving optics set-up	
Front lens focal length (mm)	600
Polarization angle (degree)	0
Polarization orientation w.r.t. scattering plane	parallel
Scattering angle (degree)	70
Scattering mode	Forward reflection
Direction of fringe motion	positive
Fringe direction angle (degree)	0
Angle adjustment (mm)	0

Experimental set-up for the photographic and the PDA studies

During the photographic and the PDA studies, the measurements were conducted in a pilot-scale impinging-jet bubble column (see Figure 2). The bubble column was made from clear acrylic and had an inside diameter of 100 mm and a total height of 1,520 mm. The column was surrounded by a 150 mm x 150 mm clear acrylic jacket that had flat surfaces and the gap between the column and the jacket was filled with clean deionized water. The outer jacket was used to minimize the distortions caused by the curved surface of the column (Mudde et al. 1997).

Extra dry air was used as the gas phase and the bubble column was operated for a period of time that was at least eight theoretical reactor hydraulic retention times before measurements were taken to allow the system to reach an isothermal steady-state condition. The pilot-scale bubble column was operated under a wide range of liquid and feed-gas flowrates. During the experiments, the liquid flowrate ranged from 6.0×10^{-5} to 2.2×10^{-4} m^{3}s^{-1} and the feed-gas flowrate ranged from 8.2×10^{-6} to 1.0×10^{-4} m^{3}s^{-1}. During the PDA and the photographic studies, measurements were conducted at a point located at the middle of the column height and at a distance equal to 1/3 of the column diameter from the column wall.

Experimental set-up for the ozonation of Kraft pulp mill effluent

The average characteristics of the raw Kraft pulp mill effluent are shown in Table 1. The ozonation tests were conducted in the extra-coarse ozone contactor (see Figure 1) as described earlier. The feed-gas flowrate ranged from 2.7×10^{-4} to 3.3×10^{-4} m^{3}s^{-1} and it contained 4.4 to 8.3 % w/w ozone. The amount of the utilized ozone ranged from 0 to 300 mgL^{-1}.

Results and Discussion

Ozonation treatment efficiencies

Extra-coarse-bubble diffuser ozone contactor

The amount of the utilized ozone (ΔO_3) for a semibatch system is defined as:

$$\Delta O_3 = \int_0^t \frac{\left(Q_{G,in}C_{G,in} - Q_{G,out}C_{G,out}\right)}{V_L} dt - C_L \qquad [2]$$

where: ΔO_3 = amount of the utilized ozone (mgL^{-1}), $C_{G,in}$ = ozone concentration in the feed gas (mgL^{-1}), $C_{G,out}$ = ozone concentration in the exhaust gas (mgL^{-1}), C_L = residual ozone concentration in the liquid phase (mgL^{-1}), V_L = effective reactor volume (m^3), $Q_{G,in}$ = feed-gas flowrate (m^{3}s^{-1}), $Q_{G,out}$ = exhaust-gas flowrate (m^{3}s^{-1}), and t = ozone contact time (s). In all the ozonation tests, the residual ozone concentration in the liquid phase was measured and found to be insignificant (< 1 %) compared to the amount of the utilized ozone. As a result, for estimating the utilized ozone doses, C_L was assumed to equal zero. Typical induced reduction efficiencies of color, AOX, COD, and TOC as functions of the amount of the utilized ozone are shown in Figure 4. On any parameter-reduction-efficiency curve, each data point represents a separate ozonation test that was conducted under certain set of operating conditions that included the feed-gas flowrate, the feed-gas ozone concentration, the pH, and the liquid and the gas-phase temperatures.
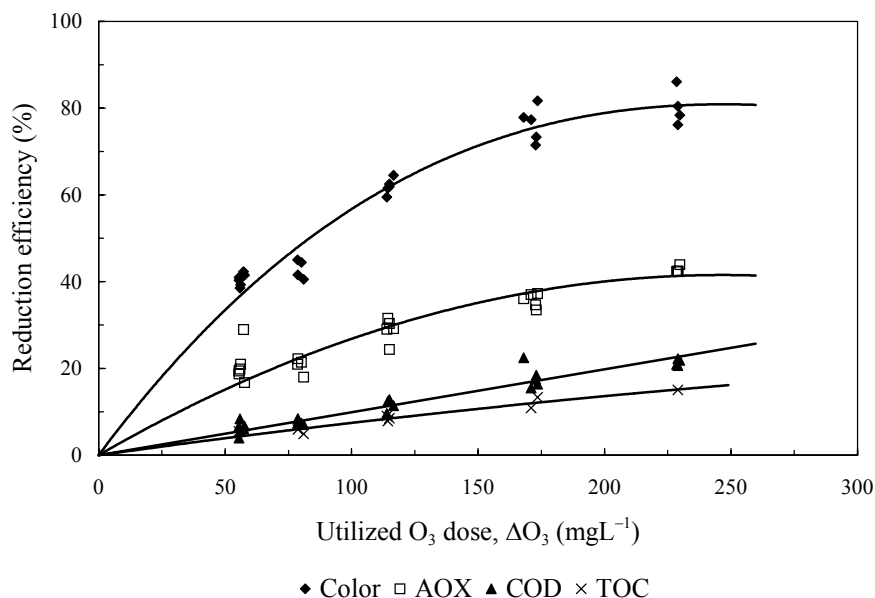
Figure 4. Reduction efficiencies of color, AOX, COD, and TOC in the extra-coarse-bubble diffuser ozone contactor.

As shown in Figure 4, the ozonation process was more effective in reducing color and AOX compared to COD and TOC. The maximum reduction efficiencies of color, AOX, COD, and TOC were 86, 44, 22, and 15 %, respectively, at ΔO_3 of 230 mgL^{-1}. These observations are consistent with the those of Zhou and Smith (1997). An explanation of this phenomenon is that the ozone has a higher selectivity towards oxidizing the easily degradable chromophoric (color-causing) and halogenated (AOX-causing) functional groups compared to the remaining organic structures.

Figure 5 shows the effect of ozonation on the BOD_5 of the Kraft pulp mill wastewater treated in the extra-coarse-bubble diffuser ozone contactor. As the amount of the utilized ozone increased, the BOD_5 of the Kraft pulp mill wastewater increased considerably by about 320 % at ΔO_3 of 230 mgL^{-1}. This phenomenon can be attributed to the reactions of ozone with the relatively recalcitrant long-chain-high-molecular-weight organic compounds that are not easily aerobically biodegradable and with the simple biodegradable organic compounds that are simultaneously present in the wastewater. The relative proportions of those organic compounds and their reaction rates with ozone determine the level of increase in the biodegradability of the wastewater (Zhou and Smith 1997). The Kraft pulp mill wastewater that is treated biologically in aerated lagoons is expected to contain larger proportions of the high-molecular-weight organic compounds since most of the easily biodegradable organic compounds have been oxidized in the biological treatment process.
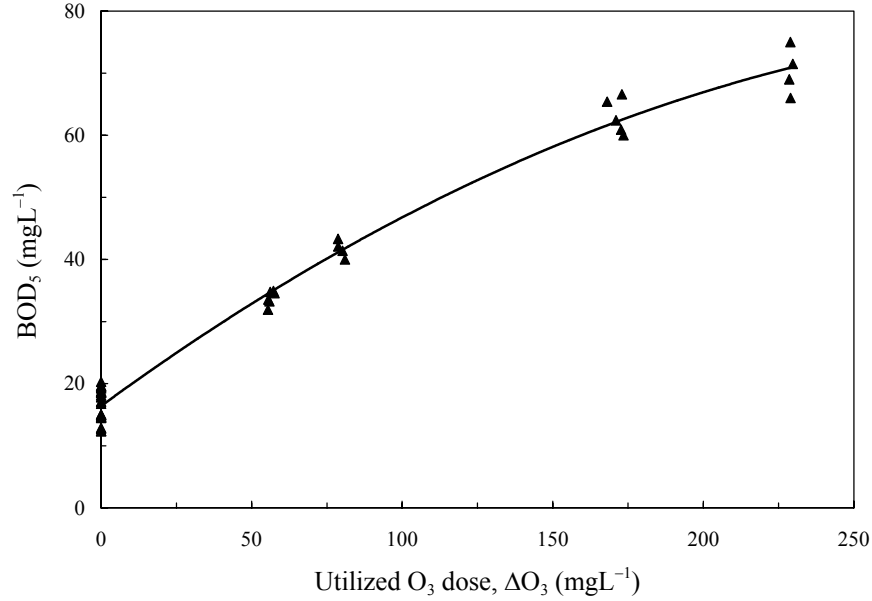
Figure 5.   The effect of ozonation on the BOD$_5$ of the pulp mill wastewater treated in the extra-coarse-bubble diffuser ozone contactor.

Impinging-jet ozone contactor

For a semibatch-flow mode, the amount of the utilized ozone can be determined using Equation 2. Meanwhile, the average amount of the utilized ozone (ΔO_3) for a continuous-flow mode is defined as:

$$\Delta O_3 = \left(\frac{Q_{G,in} C_{G,in}}{Q_L} \right) - \left(\frac{Q_{G,out} C_{G,out}}{Q_L} \right) - C_L \qquad [3]$$

where: ΔO_3 = average amount of the utilized ozone (mgL^{-1}), $C_{G,in}$ = ozone concentration in the feed gas (mgL^{-1}), $C_{G,out}$ = ozone concentration in the exhaust gas (mgL^{-1}), Q_L = liquid flowrate (m^{3}s^{-1}), $Q_{G,in}$ = feed-gas flowrate (m^{3}s^{-1}), $Q_{G,out}$ = exhaust-gas flowrate (m^{3}s^{-1}), and C_L = residual ozone concentration in the liquid phase (mgL^{-1}). For a bubble column operating in a continuous-flow mode, the amount of the utilized ozone will increase along the column height as a result of the increase in the contact time between the ozone and the fluid elements flowing through the column. Due to the relatively short liquid depth (1315 mm) inside the impinging-jet ozone contactor, it was assumed that the increase in the amount of the utilized ozone along the column height was negligible.

The reduction efficiencies of each parameter under investigation were pooled together and plotted as function of the amount of the utilized ozone. The data points, representing a wide range of the operating conditions in the injection and the ejection modes, were overlapping suggesting that there was no effect of the gas sparging mode (injection or ejection mode) on the performance of the ozonation process in terms of reducing the concentrations of color, AOX, COD, and TOC. Consequently, the oxidation efficiencies were only dependent on the amount of the utilized ozone regardless of the other process variables. As observed before, the ozonation

13

process was more effective in reducing color and AOX compared to TOC and COD. The maximum reduction efficiencies of color, AOX, COD, and TOC were 82, 72, 34, and 25 %, respectively, at ΔO_3 of 473 mgL^{-1}. At ΔO_3 of 180 mgL^{-1}, the reduction efficiencies of color, AOX, COD, and TOC were 67, 40, 8, and 11 %, respectively. When the ozone contactor was operated in a continuous-flow mode, the maximum reduction efficiencies of color, AOX, COD, and TOC were 64, 41, 12, and 20 %, respectively, at ΔO_3 of 180 mgL^{-1}. For the semibatch and the continuous-flow modes, typical curves of the ozone oxidation performance are shown in Figures 6 and 7, respectively. As the ozonation process proceeded, the performance curves of the reduction of color and AOX exhibited two distinct regions that could be identified as follows:

(1) during the initial stage of ozonation, higher and rapidly increasing reduction efficiencies occurred; then followed by
(2) gradual reduction in the treatment efficiency.

The same phenomenon was reported by several researchers (Prat and Esplugas 1989; Heinzle et al. 1992; Zhou and Smith 1997). After the initial oxidation stage, the sites that are easily oxidizable became less available for further oxidation by ozone and as a result, the competing reactions between the remaining complex organic structures and ozone became more dominant.
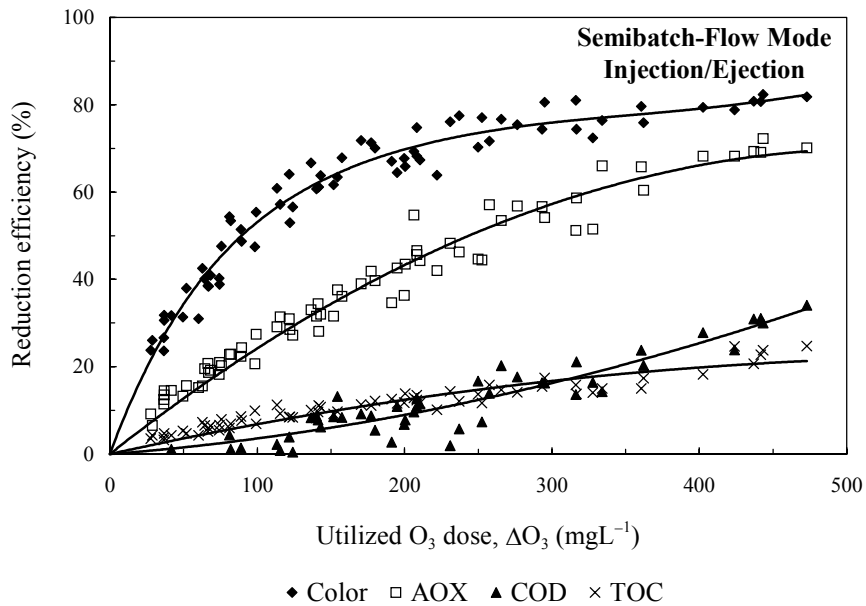

Figure 6.   Reduction efficiencies of color, AOX, COD, and TOC in the impinging-jet ozone contactor operated in a semibatch-flow mode.
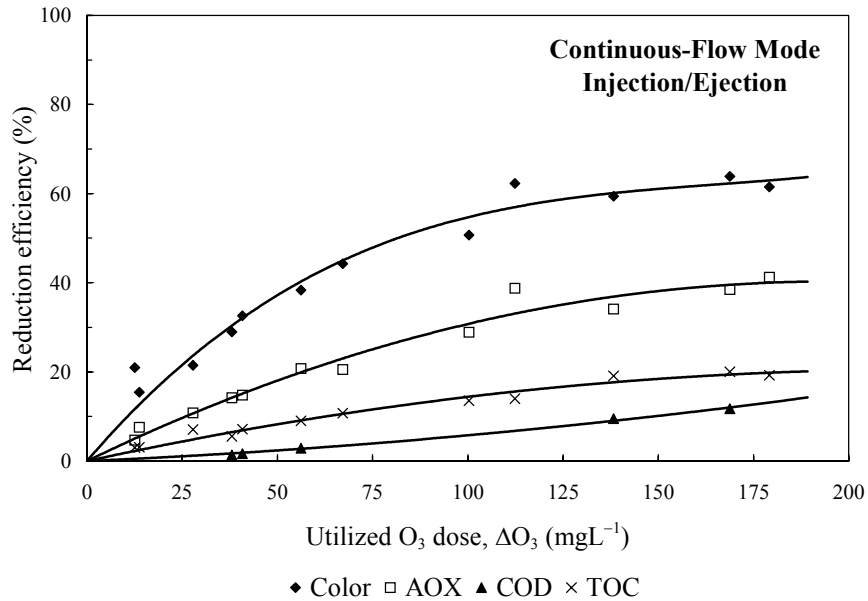
14

Figure 7.   Reduction efficiencies of color, AOX, COD, and TOC in the impinging-jet ozone contactor operated in a continuous-flow mode.
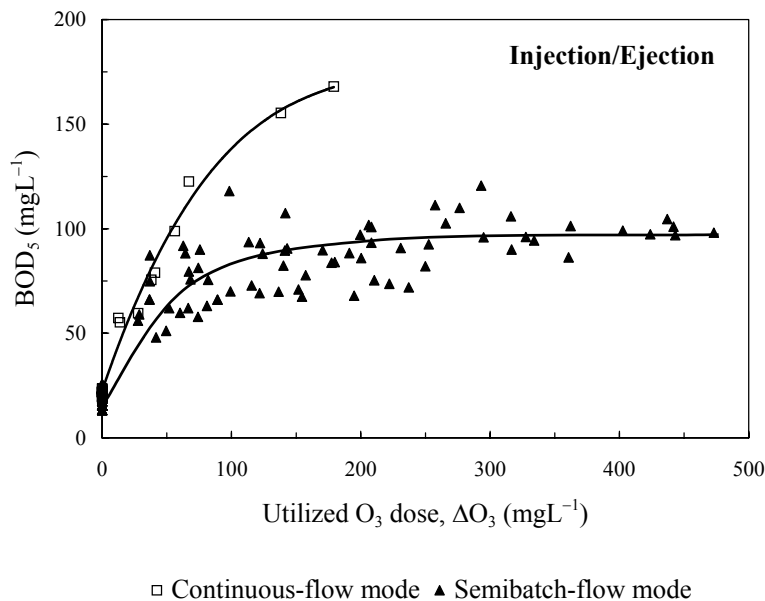

Figure 8.   The effect of ozonation on the BOD_5 of the pulp mill wastewater treated in the impinging-jet ozone contactor.

Figure 8 depicts the effect of ozonation on the BOD_5 of the Kraft pulp mill wastewater treated in the impinging-jet ozone contactor. Operating the ozone contactor in a continuous-flow mode, and as the amount of the utilized ozone increased, the BOD_5 of the pulp mill wastewater increased considerably by about 615 % at ΔO_3 of 180 mgL^{-1}. Meanwhile, in the semibatch-flow mode, the BOD_5 of the pulp mill wastewater increased by about 350 % at ΔO_3 of 180 mgL^{-1} and

by about 430 % at ΔO_3 of 473 mgL^{-1}. As shown in Figure 8 for the continuous and the semibatch-flow modes and during the initial stage of the ozonation process, a fast rate of increase of the BOD$_5$ per increase of ΔO_3 occurred. As the ozonation process proceeded, this rate started to decrease and the BOD$_5$ profile almost reached asymptote at ΔO_3 of about 180 mgL^{-1}.

Ozone gas absorption dynamics

A correction factor of 0.9 was used, as suggested by Metcalf and Eddy (1991), to correct k_La that was obtained for a clean-water ozonation system. As a result of the Kraft pulp mill effluents being highly reactive with ozone, the ozone gas absorption process was enhanced by an enhancement factor (E). Measuring the overall mass transfer coefficient (k_La) and the enhanced overall mass transfer coefficient (Ek_La) has allowed the determination of the enhancement factor of the ozone gas absorption process ($E = Ek_La/k_La$). During the ozonation experiments in all the ozone contactors, the residual ozone in the liquid phase was insignificant compared to the amount of the utilized ozone (< 1 %). Therefore, it can be reasonably assumed that at the beginning of the ozonation process, the ozone gas absorption followed the fast or instantaneous-reaction-kinetics regime. In order to determine Ek_La as a function of the amount of the utilized ozone (ΔO_3), the ozone contactors were operated in a semibatch-flow mode. In the impinging-jet ozone contactor, the gas-phase was continuously fed into the contactor through the injectors' throats while the liquid-phase was recirculated. Several assumptions were considered for the operations of the ozone contactors under semibatch-flow conditions. These assumptions can be found in Zhou and Smith (1997) and Gamal El-Din and Smith (2001). Considering an ozone contactor that is operated in a semibatch-flow mode, conducting an ozone mass balance in the gas phase, and assuming that pseudo-steady state conditions prevail at any contact time, the ozone-contactor-average Ek_La can be determined using the model developed by Zhou and Smith (1997) as follows:

$$Ek_La = \left(\frac{Q_GH}{V_L}\right)\ln\left[\frac{C_{G,in}}{C_{G,out}}\right] \qquad [4]$$

where: Ek_La = enhanced overall mass transfer coefficient (s^{-1}), Q_G = gas flowrate (m^{3}s^{-1}), $C_{G,in}$ = ozone concentration in the feed gas (mgL^{-1}), $C_{G,out}$ = ozone concentration in the exhaust gas (mgL^{-1}), V_L = effective reactor volume (m^3), and H = Henry's constant. Ek_La was calculated for each ozonation test using Equation 4 and by using the previously determined k_La, E was then calculated. Negligible accumulation of the ozone concentration in the gas phase was assumed, i.e., pseudo-steady state conditions were assumed for the gas phase as a result of the relatively small time intervals (30 s) over which the gas absorption data were analyzed.

Figure 9 represents a comparison between the fine-bubble diffuser, the extra-coarse-bubble diffuser, and the impinging-jet ozone contactors in terms of the off-gas ozone concentration profiles. The impinging-jet ozone contactor was superior to the other two contactors in terms of its higher mass transfer efficiency due to its lower off-gas ozone concentrations. Although, the impinging-jet contactor operated at higher feed-gas ozone concentrations and superficial gas velocities compared to the other two ozone contactors. When

the impinging-jet ozone contactor was operated in a continuous-flow mode, the off-gas ozone concentrations were dependent on the operating conditions encountered during the ozonation tests. The off-gas ozone concentrations were generally low in most of the experimental runs except for those that were conducted at high gas-to-liquid (G/L) flowrate ratios.
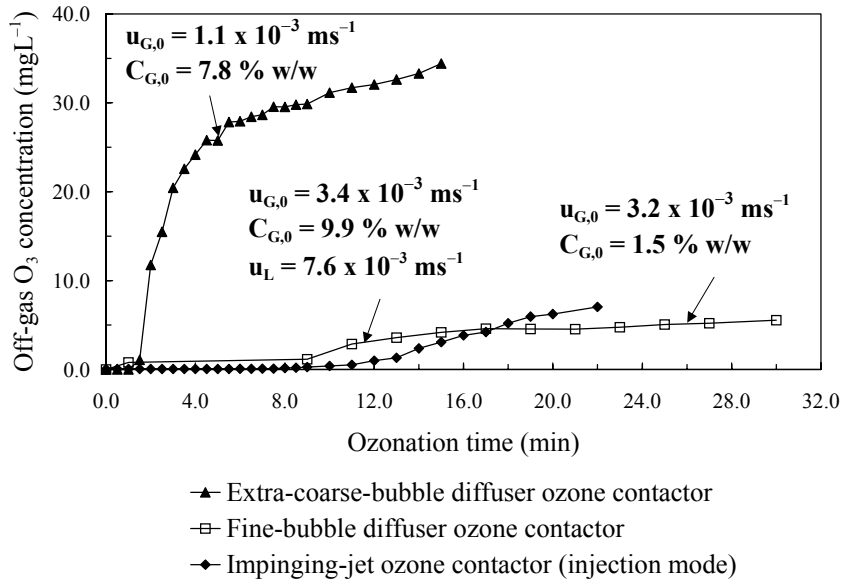

Figure 9.   The effect of ozonation on the off-gas ozone concentration profiles in three different ozone contactors operated in a semibatch-flow mode.
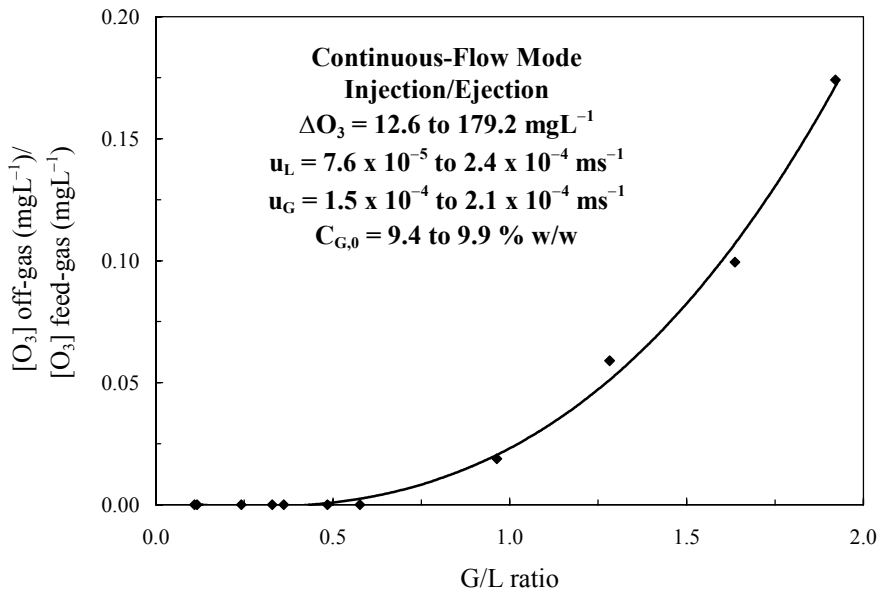

Figure 10.   The effect of ozonation on the off-gas to the feed-gas ozone concentrations' ratio in the impinging-jet ozone contactor operated in a continuous-flow mode.

The ratios of the off-gas to the feed-gas ozone concentrations were pooled for all the ozonation tests that were conducted in the injection and ejection modes and plotted together versus the G/L ratios as shown in Figure 10. Interestingly, over the wide range of the operating conditions encountered in the ozonation tests, the ratio of the off-gas to the feed-gas ozone concentrations was only a function of the G/L ratio regardless of the other process variables. The ozonation system exhibited a mass transfer efficiency of 100 % up to G/L ratio of about 0.5 then the mass transfer efficiency started to decrease and the ratio of the off-gas to the feed-gas ozone concentrations started to increase above zero as G/L ratio increased above 0.5.
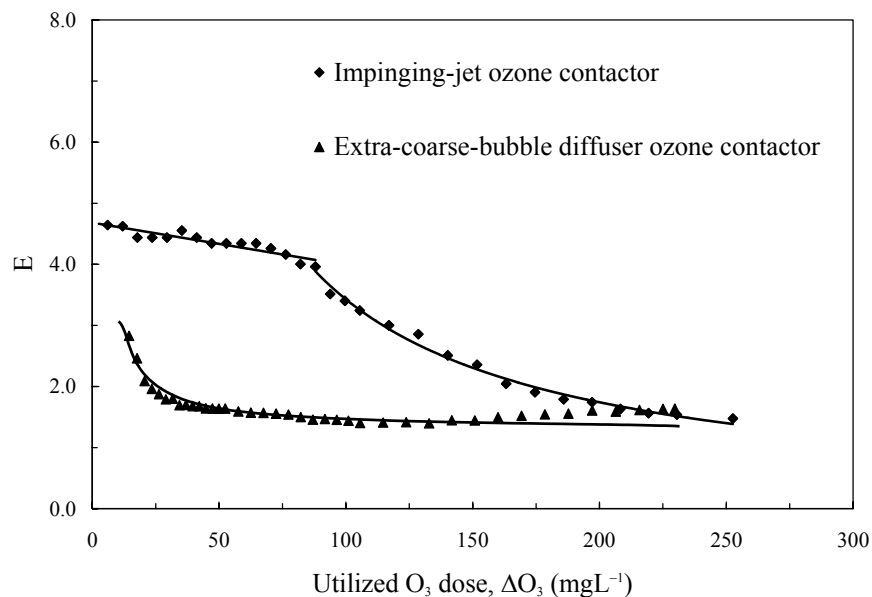

Figure 11.   The effect of ozonation on the E values in two different ozone contactors operated in a semibatch-flow mode.

Figures 11 and 12 represent typical E and ESt_G values as functions of the amount of the utilized ozone in two types of ozone contactors operated in a semibatch-flow mode. In order to compare Ek_La's obtained in contactors that had different effective reactor volumes, Ek_La was presented in terms of the dimensionless enhanced gas-phase Stanton number, ESt_G ($ESt_G = Ek_LaLRT/u_GH$). Where L is the total column height, R is the universal gas constant, T is the gas-phase temperature, and H is the Henry's constant. The operating conditions pertaining to the data presented in Figures 11 and 12 are the same as those pertaining to the data presented in Figure 9 with respect to the extra-coarse-bubble diffuser and the impinging-jet contactors. The enhancement factor (E) was higher during the initial stage of the ozonation due to the very rapid ozone reactions with the contaminants that are present in the Kraft pulp mill effluent. As the ozonation progressed, E and ESt_G decreased gradually. E and ESt_G were significantly higher in the impinging-jet contactor than in the extra-coarse-bubble diffuser contactor. In the impinging-jet contactor, two distinctive regions of this gradual decrease in E and ESt_G were observed as shown in Figures 11 and 12: an initial stage of a very small gradual linear decrease (up to almost $\Delta O_3 = 100$ mgL^{-1}); then followed by a second stage of higher gradual decrease following a

18

power-law function. The decrease in the E and ESt_G values along the course of ozonation supports the phenomenon of the shift of the ozone gas absorption process from the fast or instantaneous to the intermediate-reaction kinetics regime as the ozonation proceeds. This phenomenon was also reported before by Zhou and Smith (1997). In the impinging-jet ozone contactor, the rates of this gradual decrease in ESt_G and E with the increase in the amount of the utilized ozone were much lower, especially at the beginning of the ozonation process, than those observed in the extra-coarse-bubble diffuser contactor. This observation along with the low off-gas ozone concentrations produced in the impinging-jet ozone contactor have proved that this ozone contactor can provide a more efficient contacting technology for treating Kraft pulp mill effluents as compared to the conventional diffuser ozone contactors.
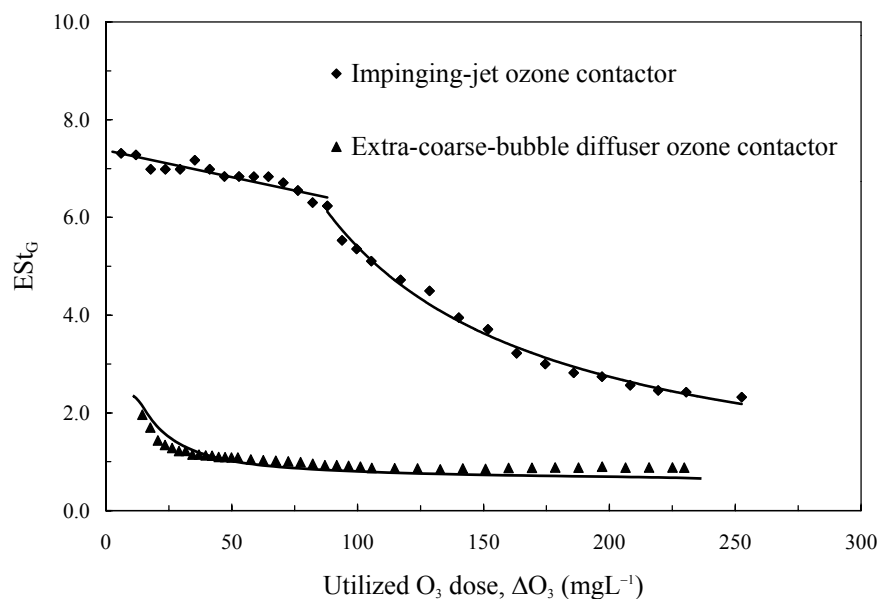

Figure 12. The effect of ozonation on the ESt_G values in two different ozone contactors operated in a semibatch-flow mode.

Modeling of the ozonation treatment efficiencies

Figures 10.12 to 10.15 depict typical plots of the BOD_5/COD, color/COD, AOX/COD, and TOC/COD concentrations' ratios as functions of ΔO_3. The solid lines in Figures 10.12 to 10.15 represent the general trends in the change in the BOD_5/COD, color/COD, AOX/COD, and TOC/COD concentrations' ratios as functions of ΔO_3. The relative ratio between the concentrations of the recalcitrant long-chain-high-molecular-weight organic compounds that are not easily aerobically biodegradable and the simple biodegradable organic compounds determines the effectiveness of the ozonation process in increasing the biodegradability of the Kraft pulp mill wastewater. It is more accurate to represent the biodegradability of the wastewater as a ratio of BOD_5 to COD. As shown in Figure 13, ozonation has caused the biodegradability (represented by BOD_5/COD) of the Kraft pulp mill wastewater treated in the impinging-jet ozone contactor to increase from 0.03 to 0.22 at ΔO_3 up to 473 mgL^{-1}. The small ratio of the final BOD_5/COD indicates the need for further treatment of the Kraft pulp mill

wastewater to increase its biodegradability, and consequently, to remove the increase in the BOD_5 of the wastewater as a result of applying further treatment. One of the promising treatment options that can be investigated is the combination of hydrogen peroxide and ozone treatment followed by a biological treatment process.
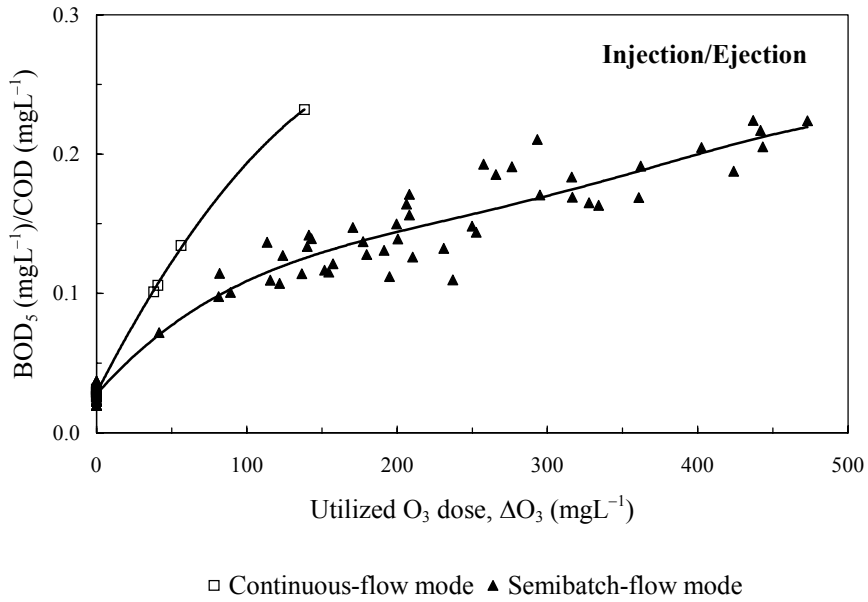

□ Continuous-flow mode ▲ Semibatch-flow mode

Figure 13.   The effect of ozonation on the BOD_5/COD ratio of the treated Kraft pulp mill wastewater in the impinging-jet ozone contactor.

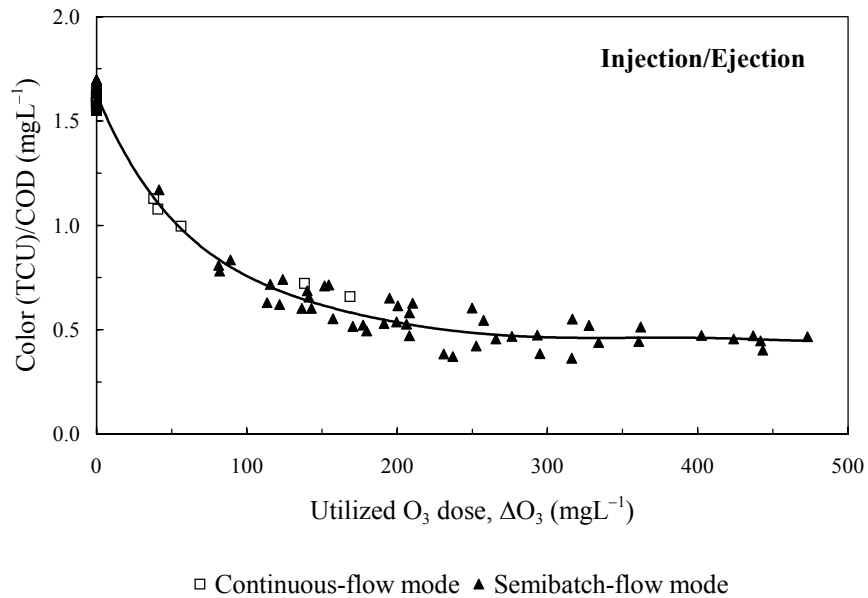□ Continuous-flow mode ▲ Semibatch-flow mode

Figure 14.   The effect of ozonation on the color/COD ratio of the treated Kraft pulp mill wastewater in the impinging-jet ozone contactor.

The color/COD ratios of the Kraft pulp mill wastewater that was treated in the continuous and the semibatch-flow modes under a wide range of operating conditions were pooled together and plotted versus ΔO_3 as shown in Figure 14. There was no effect of the operating mode on the ozonation treatment levels. For the AOX/COD and TOC/COD ratios, as shown in Figures 15 and 16, the same trend in the reduction of those ratios was observed in the continuous and the semibatch-flow modes except that the initial values (at $\Delta O_3 = 0$) of those ratios were lower in the experiments conducted in the continuous-flow mode. The COD decrease along the course of ozonation was well represented by a linear function that had the same slope for both the continuous and the semibatch-flow modes. In order to achieve accurate modeling of the ozonation treatment efficiencies in terms of the color, AOX, COD, and TOC induced reduction efficiencies, the ratio of the initial concentration of the parameter, under investigation, to the initial COD concentration in the pulp mill wastewater can be introduced as another parameter that affects the ozonation treatment levels. This ratio represents the effects of the competing reactions between ozone and the various constituents that are present in the Kraft pulp mill wastewater during the course of ozonation.
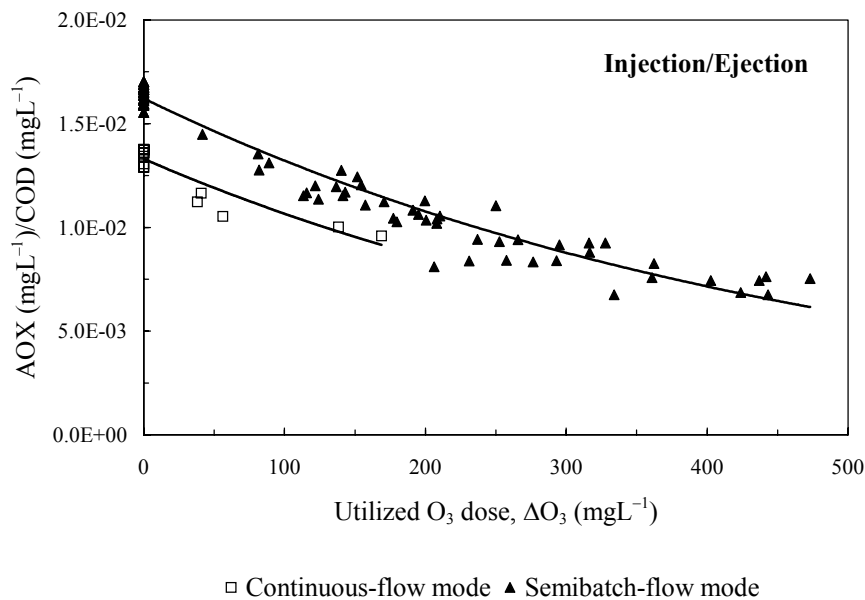

Figure 15.   The effect of ozonation on the AOX/COD ratio of the treated Kraft pulp mill wastewater in the impinging-jet ozone contactor.

A general model that can describe the performance of the ozonation treatment can be represented as follows:

$$\log\left(\frac{Y}{Y_0}\right) = a \cdot \Delta O_3 + b \cdot \Delta O_3 \cdot \log\left(\frac{Y_0}{COD_0}\right) \qquad [5]$$

This model can be applied to describe the ozonation process reduction efficiencies of color, AOX, and TOC. For COD reduction, the term $\log(Y_0/COD_0)$ reduces to zero. As a result, Equation 5 becomes:

$$\log\left(\frac{Y}{Y_0}\right) = a \cdot \Delta O_3 \qquad [6]$$

where: Y = final wastewater characteristic parameter concentration (TCU for color, and mgL^{-1} for AOX, COD, and TOC), Y_0 = initial wastewater characteristic parameter concentration (TCU for color, and mgL^{-1} for AOX, COD, and TOC), ΔO_3 = amount of the utilized ozone (mgL^{-1}), COD_0 = initial wastewater COD concentration (mgL^{-1}), and a and b are empirical regression constants. Similar models to those represented by Equations 5 and 6 were developed before by Zhou and Smith (2000a).

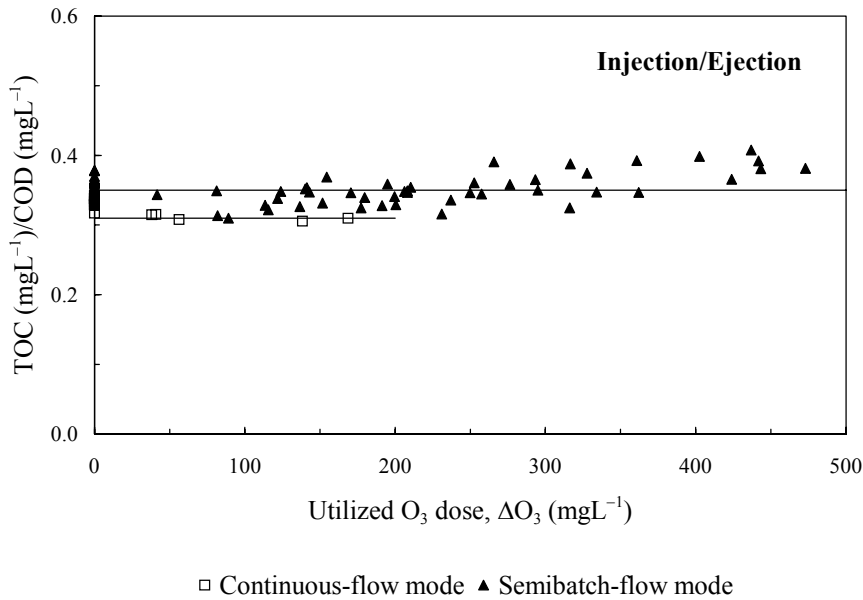□ Continuous-flow mode ▲ Semibatch-flow mode

Figure 16.   The effect of ozonation on the TOC/COD ratio of the treated Kraft pulp mill wastewater in the impinging-jet ozone contactor.

The experimental data representing the induced reduction efficiencies of color, AOX, COD, and TOC that were obtained in the continuous and the semibatch-flow modes were pooled together and linear regression analyses were performed to obtain the regression constants (a and b) for each parameter under investigation and finally to examine the applicability of the models represented by Equations 5 and 6 in predicting the ozone induced reductions of color, AOX, COD, and TOC. The same procedure was performed for the data obtained in the extra-coarse-bubble diffuser ozone contactor. The regression analyses was performed at a 95 % confidence level and the constant parameter was set equal to zero in order to account for the no-treatment condition when the amount of utilized ozone is equal to zero. The regression analyses produced coefficients of multiple correlation (R's) in the range of 0.89 to 0.97 for the data obtained in the extra-coarse-bubble diffuser ozone contactor and in the range of 0.79 to 0.98 for the data obtained in the impinging-jet ozone contactor.
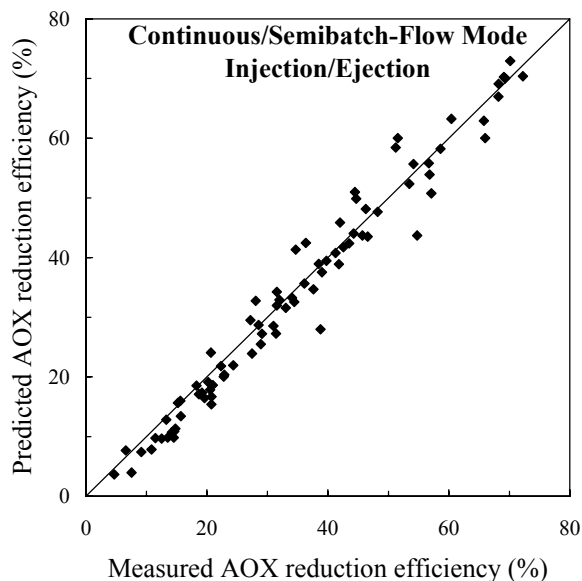
Figure 17.　A comparison between the predicted and the measured reduction efficiencies of AOX.

Table 3.　Regression parameters for the modeling of the induced reduction efficiencies of color, AOX, COD, and TOC

Wastewater parameters	Estimated parameters		Multiple R value
	a	b	
Extra-coarse ozone contactor			
Color	-1.88E-03	-6.91E-03	0.95
AOX	-8.15E-03	-3.78E-03	0.89
TOC	-4.35E-04	-2.68E-04	0.97
COD	-4.74E-04	N/A	0.96
Impinging-jet ozone contactor			
Color	-4.06E-03	9.04E-03	0.81
AOX	2.92E-04	8.39E-04	0.98
TOC	8.64E-05	7.87E-04	0.79
COD	-2.79E-04	N/A	0.88

The regression parameters obtained for all the wastewater quality parameters representing the Kraft pulp mill wastewater that was treated in the impinging-jet and the extra-coarse-bubble diffuser ozone contactors are shown in Table 3. A Comparison between the predicted and the measured induced ozone reduction efficiencies of the AOX of the Kraft pulp mill wastewater that was treated in the impinging-jet ozone contactor, under various amounts of the utilized ozone, is shown in Figure 17.

Scale-up of the ozonation process

Different ozone contactor designs and configurations should be tested over a wide range of operating conditions in order to achieve proper scale-up of the ozonation process for treating Kraft pulp mill wastewaters. Consequently, relationships can be developed to predict the ozonation treatment levels that can be achieved when scaling up ozone contactors. Zhou and Smith (1997, 2000a) investigated the factors that would influence the scale-up of conventional fine-bubble diffuser ozone contactors. They tested their unit in two operating modes: the semibatch and the continuous-flow modes. Also, two contactor sizes were tested: 6.0×10^{-2} m^3 and 4.0×10^{-3} m^3. Detailed description of their experimental protocols can be found in Zhou and Smith (1997, 2000a). They reported that there was a small scale-up factor associated with the ozonation treatment of Kraft pulp mill wastewaters, although, there was no effect of the mode of operations on the induced reductions of color, AOX, COD, and TOC.

Table 4. A comparison between three different scales and designs of ozone contactors in terms of the color, AOX, COD, and TOC reduction efficiencies

Operating conditions	Ozone contactor # (1)	Ozone contactor # (2)	Ozone contactor # (3)	Ozone contactor # (4)
Mode of operations	semibatch	semibatch/ continuous	semibatch	semibatch/ continuous
Gas sparging technique	extra-coarse diffuser	impinging gas-liquid jets	fine diffuser	fine diffuser
Reactor volume (m^3)	2.1×10^{-1}	1.7×10^{-2}/ 1.0×10^{-2}	4.0×10^{-3}	6.0×10^{-2}/ 7.0×10^{-2}
Reactor aspect ratio	1.6	13.2	5.4	22.3/31.3
ΔO_3 (mgL^{-1})	125	125	125	125
Wastewater parameters	**% Reduction efficiencies**			
Color	65	60	75	63
AOX	31	35	52	32
COD	12	17	20	19
TOC	10	9	17	10

Furthermore, a comparison was conducted between the two scales of fine-bubble diffuser ozone contactors used by Zhou and Smith (1997, 2000a) and the ozone contactors used in the current study in terms of the ozonation treatment levels at a similar ΔO_3 of 125 mgL^{-1}. The ozonation induced reduction efficiencies in the four ozone contactors designs are shown in Table 4. The results indicated that the scale-up and reactor configuration have exhibited insignificant effects

on the ozonation treatment efficiencies. Despite that the impinging-jet ozone contactor, as discussed earlier, has shown to produce lower off-gas ozone concentrations compared to the other ozone contactors that were operated in a semibatch-flow mode. The treatment levels achieved in the impinging-jet and fine-bubble diffuser ozone contactors that were operated in a continuous-flow mode were compared. The two designs of ozone contactors have produced almost identical treatment levels except that the volume of the impinging-jet contactor was one seventh of that of the fine-diffuser contactor. Consequently, the operating costs of the ozonation process and the ozone off-gas destruction facilities will be greatly reduced when the impinging-jet ozone contactor is used for treating Kraft pulp mill wastewaters.
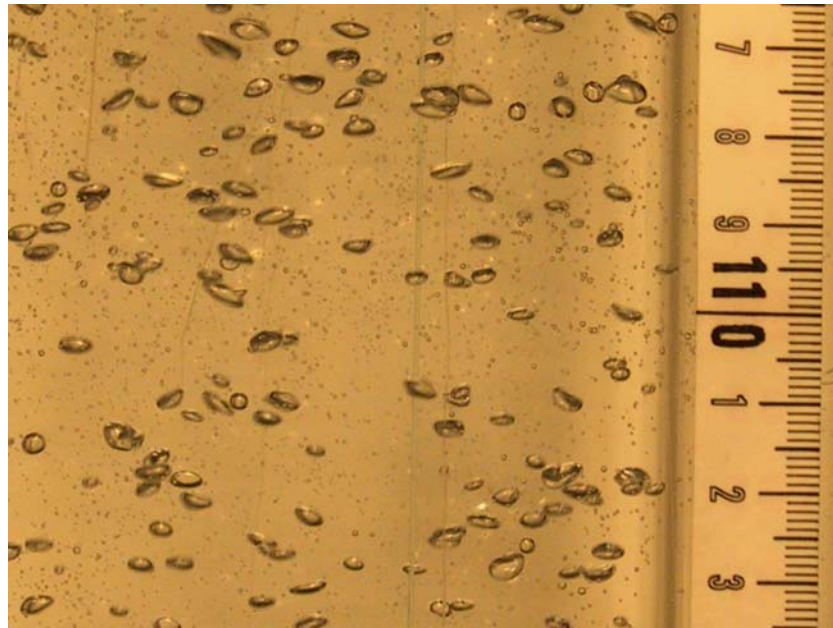

Figure 18.   A digital image of the air bubbles at u_L = 7.7 x 10^{-3} ms^{-1} and u_G = 1.0 x 10^{-3} ms^{-1}.

Gas bubble measurements
Digital photographic measurements
        The rise velocity of bubble swarms was measured to be in the range of 2.4 x 10^{-1} to 3.0 x 10^{-1} ms^{-1}. Similar ranges of bubble rise velocity were obtained by several researchers who investigated the hydrodynamics of gas bubbles in air-water systems (Kaštánek et al. 1993). The photographic images revealed that the majority of the bubbles had an oblate ellipsoidal shape as shown in Figures 18 to 20. Therefore, the bubble diameter (d_B) was calculated as the arithmetic mean of the maximum and minimum diameters of the bubbles. The angle between the major axis of the bubble and the horizontal direction was generally ≤ 90°.

        For all operating conditions, the mean d_B ranged from about 1,400 μm to 2,200 μm and an increase in u_G caused d_B to increase while an increase in u_L caused d_B to decrease. Yamashita et al. (1978) observed in their photographic study of the gas bubbles in an air-water system that although most of the bubbles were oblate ellipsoids rather than spheroids, d_S and d_B were almost

identical. Therefore, it can be reasonably assumed that d_B obtained in the current photographic study is an indicator of, if not equal to, d_S.
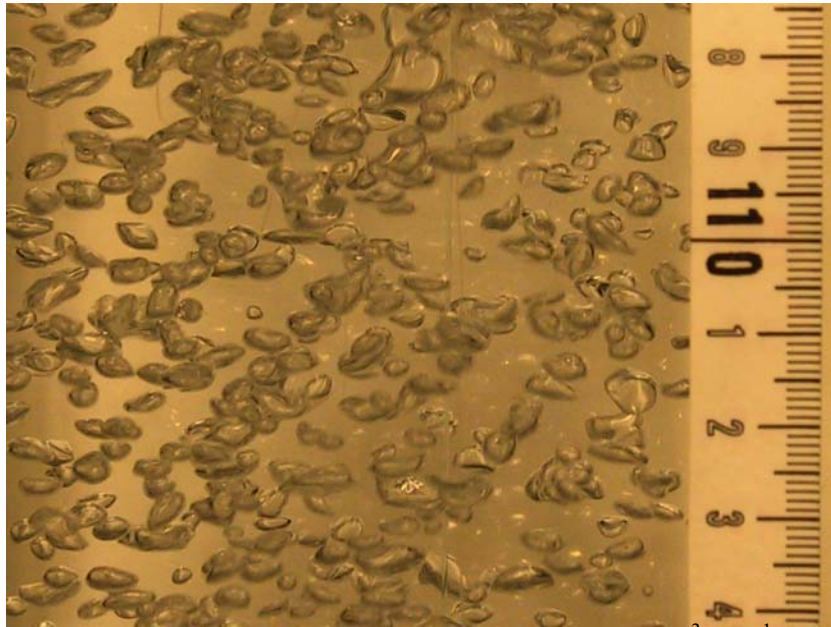

Figure 19.   A digital image of the air bubbles at $u_L = 7.7 \times 10^{-3}$ ms^{-1} and $u_G = 7.8 \times 10^{-3}$ ms^{-1}.

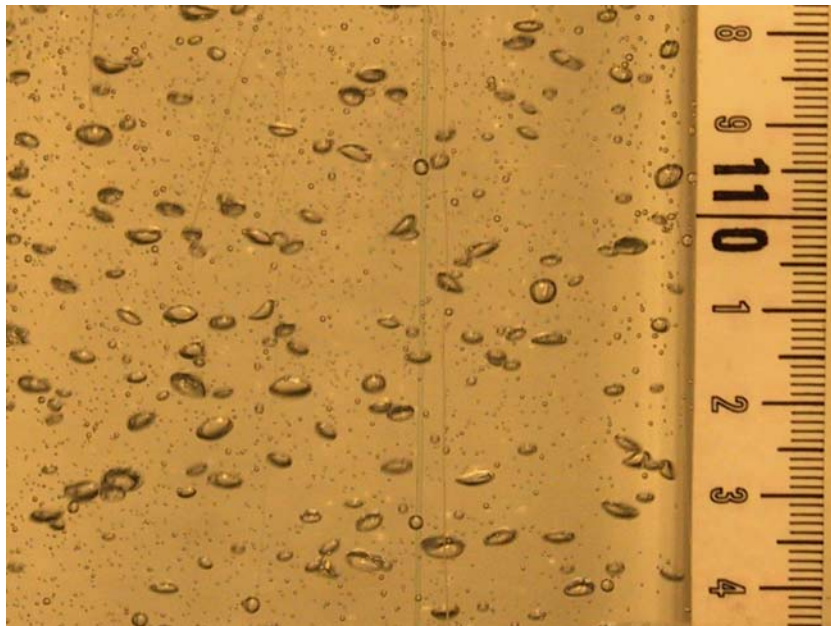Figure 20.   A digital image of the air bubbles at $u_L = 1.9 \times 10^{-2}$ ms^{-1} and $u_G = 8.7 \times 10^{-4}$ ms^{-1}.

Particle dynamics analyzer measurements in deionized water

Figure 21 depicts the effects of the superficial gas and liquid velocities (u_G and u_L, respectively) on the count mean and Sauter mean bubble diameters (d_B and d_S, respectively). The gas phase was sparged under positive pressure, i.e., in the injection mode. As shown in Figure 8, at $u_G \leq 4.0 \times 10^{-3}$ ms^{-1} and as u_L increased, the rate of decrease in d_B per increase in u_G was lower than that at $u_G \geq 4.0 \times 10^{-3}$ ms^{-1}. At $u_G \geq 4.0 \times 10^{-3}$ ms^{-1}, the rate of decrease in d_B per increase in u_G was almost the same for different u_L's. A similar phenomenon was observed by Zhou and Smith (2000b). Meanwhile, as u_L increased, d_S decreased. Alternatively, as u_G increased, d_S increased almost proportionally as observed before in the study of Unno and Inoue (1980) that involved measurements of the sizes of bubbles produced from an orifice mixer that was placed at the bottom of a bubble column. In the impinging-jet bubble column, it was observed that as u_L increased, the turbulence intensity and turbulent shear stresses increased.
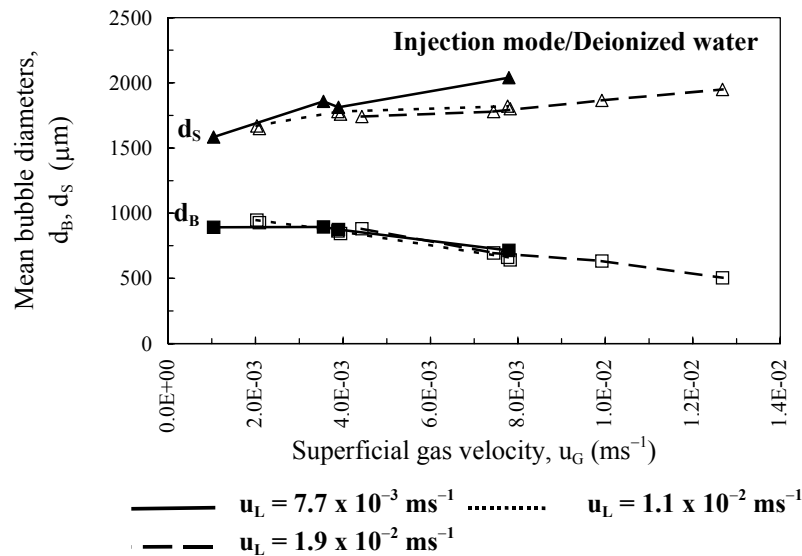

Figure 21. Effects of u_G and u_L on d_B and d_S in deionized water.

Consequently, this resulted in higher shearing of the large gas bubbles into smaller bubbles. Therefore, the mean d_B and d_S decreased and they were smaller than those observed before in the studies of Zhou and Smith (2000b) and Roustan et al. (1996) that were conducted in conventional bubble columns. As indicated earlier by the photographic study, most of the bubbles were ellipsoids rather than spheroids. Therefore, the value of d_B, obtained in the PDA study, was dependent on the local curvature of the scattering surface of the bubble and the orientation of the bubble with respect to the optical measurement volume. The same observation was reported before by Stanley and Nikitopoulos (1996) when they investigated the effects of the hydrodynamics of an upward gas-liquid jet on the bubble size. Therefore, the value of d_B, obtained in the PDA study, is not a true measure of the actual count mean bubble diameter of an oblate ellipsoidal bubble. The value of d_B, obtained in the PDA study, ranged from 500 to 950 µm. Under similar operating conditions to those used in the photographic study, the value of d_S,

obtained in the PDA study, ranged from 1,585 to 2,040 μm. These values were in good agreement with those obtained in the photographic study. Similar trends were observed when the gas phase was sparged under vacuum or negative pressure, i.e., in the ejection mode.
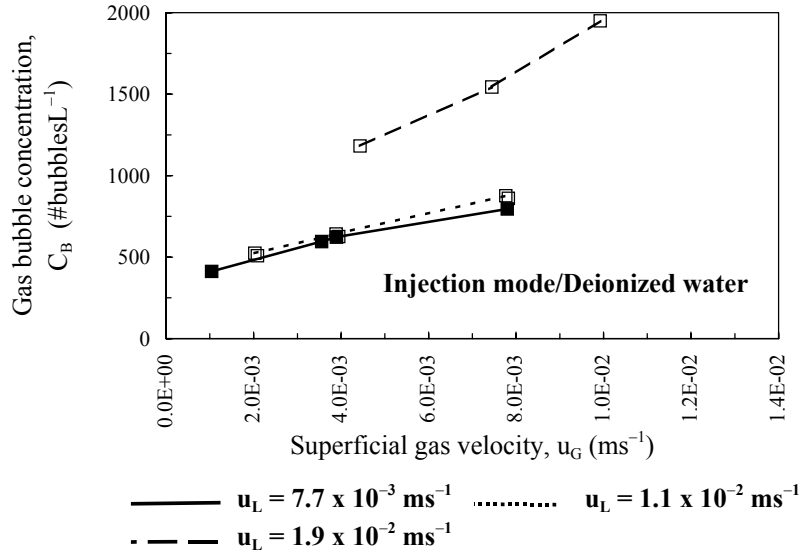

Figure 22.   Effects of u_G and u_L on C_B in deionized water.

The effects of u_G and u_L on the concentration of the bubbles (C_B) are shown in Figure 22. C_B increased almost proportionally with the increase in u_G and u_L. The rate of increase in C_B per increase in u_L was higher than the rate of increase in C_B per increase in u_G. This could have been a result of a high shearing of the large gas bubbles caused by the increase in u_L. Similar trends were observed during the experiments conducted in the ejection mode.

During the experiments conducted in the injection mode and as shown in Figure 23, it was observed that the gas-phase turbulence % in the axial direction (i.e., the root mean square (RMS) velocity divided by the mean axial velocity) increased almost linearly as u_G increased. Meanwhile as u_L increased from 7.7×10^{-3} to 1.9×10^{-2} ms^{-1} and at $u_G \leq 4.5 \times 10^{-3}$ ms^{-1}, the turbulence % in the axial direction generally increased. Although the turbulence intensity in the liquid phase was not measured, it was expected that since the turbulence levels in the gas phase were high, the liquid phase would as well exhibit high levels of turbulence. The increase in turbulence % could be a result of the gas-liquid flow being in the bubbly flow regime due to the low u_G encountered in this range of operating conditions. The latter phenomenon could be a result of the decrease in the Sauter mean diameter of the bubbles, and consequently, that could have caused an increase in the entrainment of the surrounding liquid by the rising gas bubbles that carried the entrained liquid upwards. Therefore, the circulation flow pattern could have increased and caused more turbulence in the dispersed flow. At $u_G \geq 4.5 \times 10^{-3}$ ms^{-1}, the turbulence % in the axial direction decreased gradually as u_L increased. This could be a result of the gas-liquid flow approaching a homogeneous bubbly flow regime that is usually characterized

by its high bubble concentration. Also, a somewhat uniform bubble rise velocity distribution was observed. This could have led to rising of the bubbles without much of mutual bubble interferences, thus, leading to somewhat uniform degrees of axial and radial distribution of gas hold-up and a low degree of turbulence in the axial direction. Similar phenomenon was reported by (Kaštánek et al. 1993). The gas sparging mode had no effect on the dependency of turbulence % on u_G and u_L.
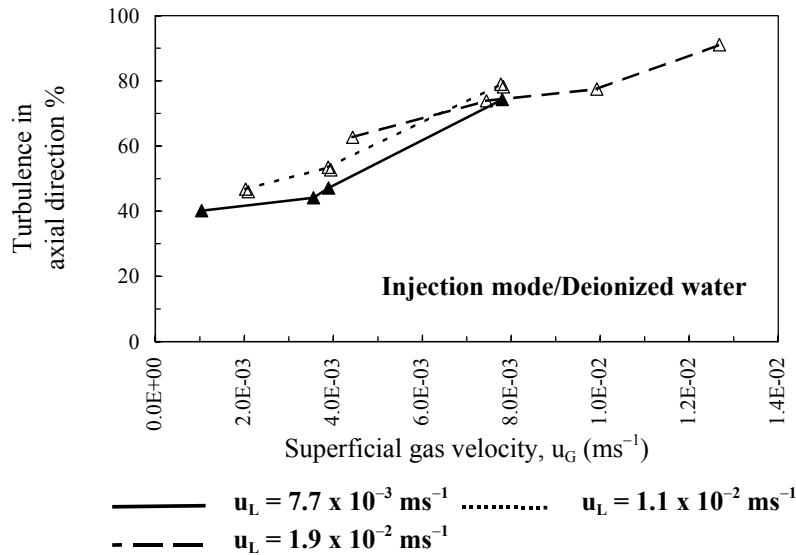

Figure 23.   Effects of u_G and u_L on the gas-phase axial turbulence % in deionized water.

Figure 24 depicts typical plots of the probability density distributions of the axial bubble rise velocity (u) as well as the radial velocity (v) for two different tests (TR8 and TR10) that were conducted in the injection mode (i.e., the gas phase was sparged under positive pressure). TR8 was conducted at u_L of 7.7 x 10^{-3} and u_G of 3.9 x 10^{-3} ms^{-1} while, TR10 was conducted at u_L of 1.9 x 10^{-2} and u_G of 4.4 x 10^{-3} ms^{-1}. The velocity profiles were normally distributed as shown in Figure 24. The mean radial velocity (v) was 1.2 x 10^{-3} and 1.1 x 10^{-3} ms^{-1} in TR8 and TR10, respectively. The radial velocity profiles confirmed the existence of a circular flow pattern in the bubble column as suggested before by Deckwer (1992). The circular flow pattern is a result of the liquid phase dispersion caused by the entrainment of the surrounding liquid by the rising gas bubbles that carry the entrained liquid upwards (Deckwer 1992). The mean axial bubble rise velocity (u) was 3.1 x 10^{-1} and 2.9 x 10^{-1} ms^{-1} in TR8 and TR10, respectively. Since u_G was almost constant between the two runs and as u_L increased, u decreased and the spread of the profile was narrowed. In the impinging-jet bubble column, it was observed that as u_L increased, the gas-phase axial turbulence % increased (at $u_G \leq$ 4.5 x 10^{-3} ms^{-1}) causing the turbulent shear stresses to increase considerably. Consequently, this resulted in higher shearing of the large gas bubbles into smaller bubbles, i.e., smaller d_B and as a result, u decreased. Similar trends were observed during the experiments conducted in the ejection mode.
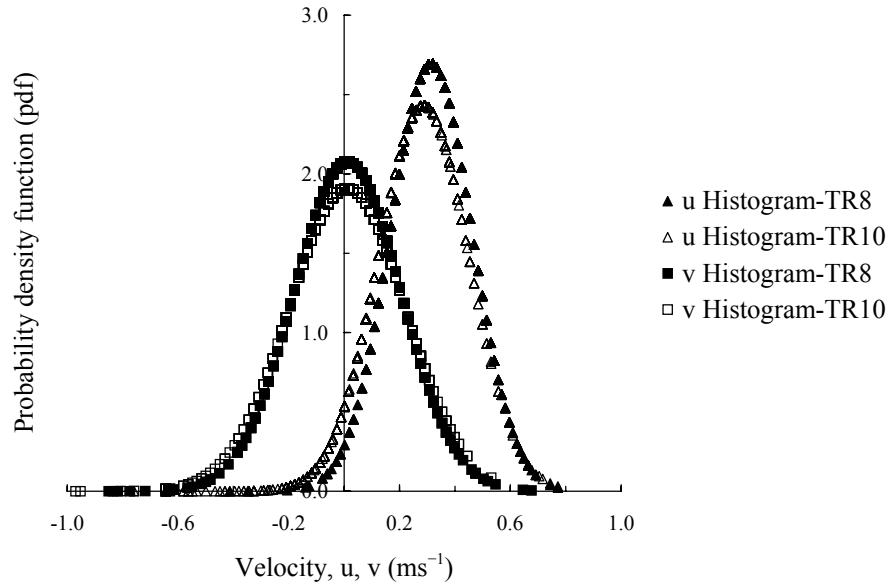
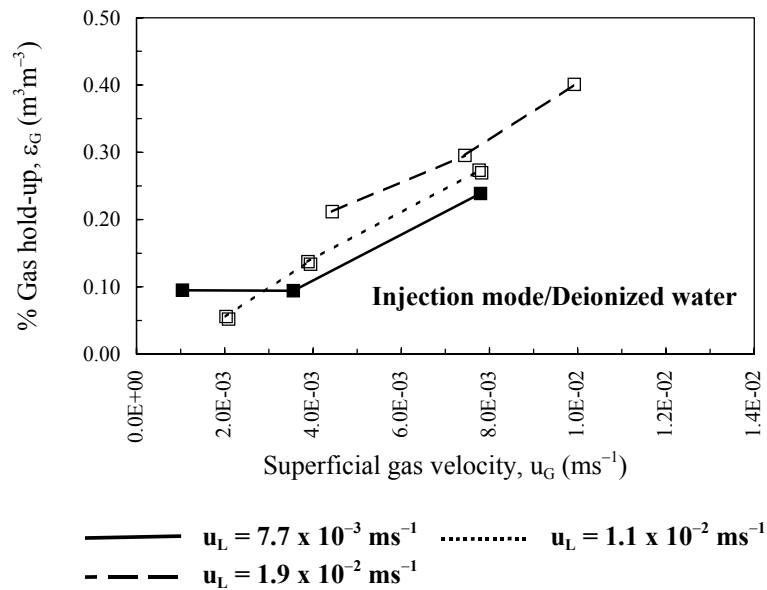Figure 24.   Typical probability density distributions of the gas-phase u and v in deionized water.

Figure 25.   Effects of u_G and u_L on ε_G in deionized water.

Figure 25 presents the effects of u_G and u_L on the gas hold-up (ε_G). The gas hold-up was estimated based on the bubble concentration (C_B) and the count mean bubble diameter (d_B) measurements. As shown in Figure 17, ε_G increased proportionally with the increase in u_G as reported before by several researchers (Deckwer 1992; Kaštánek et al. 1993; Roustan et al. 1996; Zhou and Smith 2000b). This phenomenon was a result of the decreased bubble size as u_G and u_L increased, and thus, leading to a longer bubble residence time in the bubble column. Also, as u_L

increased, an increase in ε_G occurred due to the smaller bubble size that resulted from the increase in the shearing of the large gas bubbles into smaller bubbles. An increase in u_G and u_L led to a proportional increase in the gas bubbles' interfacial area (a). This could be a result of the increase in ε_G as u_G and u_L increased. The same phenomenon was reported by (Zhou and Smith, 2000b). Once more, there was no observed effect of the gas sparging mode on the dependency of ε_G and a on u_G and u_L.

Particle dynamics analyzer measurements in Kraft pulp mill effluent

Kraft pulp mill effluents contains surfactants, or referred to as surface active agents (SAA's), and other organic and inorganic compounds that can affect the liquid viscosity and the bubble surface tension. These effects depend on the type, concentration, and chemical structure of such compounds. The organic compounds can be divided into two main groups (Voigt and Schügerl 1979): polar organic compounds with low molecular weight; and polar organic compounds with high molecular weight. The SSA's tend to accumulate at the gas-liquid interface with their hydrophobic groups positioned towards the gas phase (Zhou and Smith 2000b). As a result, the surface tension at the interface will be lower than the surface tension in the bulk liquid. Therefore, the surface tension gradient across the liquid film, surrounding the gas bubble, will be higher than that in the bulk liquid leading to a decrease in the size of the gas bubbles. Also, the SAA's can cause damping of the turbulence intensity at the gas-liquid interface and that will lead to a suppression of the coalescence of the mutually contacting gas bubbles (Kaštánek et al. 1993). The coalescence suppressing effect is smallest during the bubble formation and increases as the contact time between the gas phase and the liquid phase increases (Voigt and Schügerl 1979). The higher the molecular weight of the polar organic compounds, the stronger the suppression of the coalescence but the longer it takes the coalescence suppressing effect to increase as the age of the bubble increases inside the bubble column. In contrast to the SAA's, the inorganic (i.e., salt) compounds exhibit a different effect on the coalescence suppression (Voigt and Schügerl 1979). In inorganic solutions, the concentration of the salt compounds in the bulk liquid is the same as that at the gas-liquid interface. This is a result of the liquid phase immediately forming a liquid film around the gas bubble following the bubble formation, therefore, the gradient in the salt concentration between the bulk liquid and at the gas-liquid interface begins to decrease over time. As a result, the salt compounds have their maximum coalescence suppressing effect at the initial stage of the bubble formation and this effect starts to decrease as the age of the gas bubble inside the bubble column increases (Voigt and Schügerl 1979).

Regarding the effects of the superficial gas and liquid velocities (u_G and u_L, respectively) on the count mean bubble diameter (d_B), the Sauter mean bubble diameter (d_S), the gas bubble concentration (C_B), the gas-phase axial turbulence intensity, the gas bubble rise velocity (u), the gas hold-up (ε_G), and the specific gas bubble interfacial area (a), similar trends of those effects were observed when the PDA measurements were conducted during the aeration of the raw Kraft pulp mill effluent as well as the ozonated effluent. The effects of u_G and u_L on d_B and d_S during the aeration of raw Kraft pulp mill effluents (i.e., $\Delta O_3 = 0.0$ mgL^{-1}) are shown in Figure 26. As u_G increased, the Sauter mean diameter increased at a rate similar to that observed during the

aeration experiments conducted in the deionized water. Also, as u_L increased, d_S decreased at a rate similar to that observed in the deionized water. Interestingly, during the aeration of the raw Kraft pulp mill effluent, and as u_G increased, d_B increased slightly then it started decreasing. This phenomenon could be a result of the low coalescence suppressing effect of the SAA's due to the short gas bubble residence time in the column that resulted from the increase in the bubble rise velocity (u) as u_G increased up to 4.0 x 10^{-3} ms^{-1}.
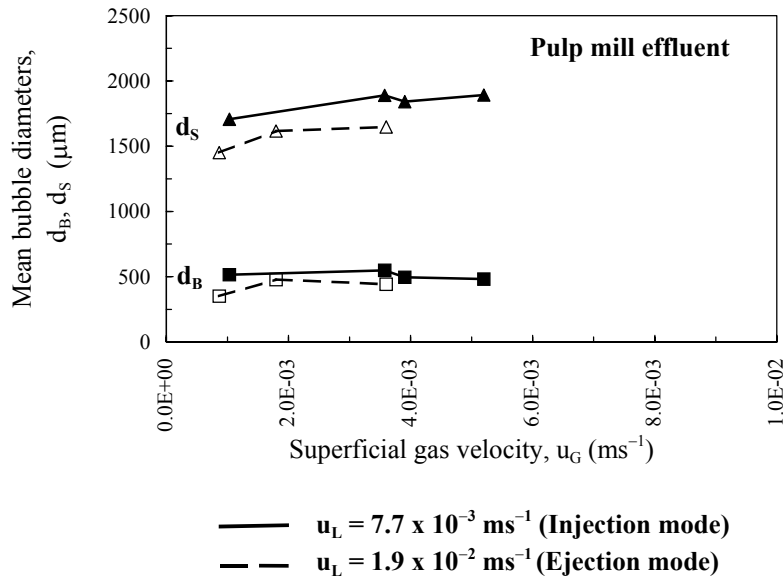

Figure 26.   Effects of u_G and u_L on d_B and d_S in raw Kraft pulp mill effluent.

As observed during the aeration of the deionized water and at u_G > 4.0 x 10^{-3} ms^{-1}, u started to decrease and that led to an increase in the gas bubble residence time. Consequently, that might have led to an increase in the coalescence suppressing effect of the SAA's, and thus, causing d_B to decrease. Alternatively, during the aeration of the ozonated Kraft pulp mill effluents, the effect of u_G on d_B was similar to that observed in the deionized water. Generally, the effect of increasing u_L on decreasing d_B, during the aeration of the raw and the ozonated Kraft pulp mill effluents, was higher than that observed during the aeration of deionized water. This effect gradually decreased as the amount of the utilized ozone (ΔO_3) increased, possibly due to the increase in the partial or complete oxidation and/or destruction of the surfactants and the inorganic compounds that were present in the raw Kraft pulp mill effluent. The measured d_B and d_S in the raw and ozonated Kraft pulp mill effluents were smaller than those obtained in conventional diffuser bubble columns that were tested in the study of Zhou and Smith (2000b).

The effects of ΔO_3 on d_B and d_S, for one set of u_G and u_L in the injection mode, are presented in Figure 27. As ΔO_3 increased from 0 to 300 mgL^{-1}, d_S increased by almost 8 % (from 1,840 to 1,990 μm) and d_B increased by almost 41 % (from 495 to 700 μm). As shown in Figure 27, d_S was virtually identical in both the deionized water and the raw Kraft pulp mill

effluent. Meanwhile, d_B in the deionized water was almost two times larger than that in the raw Kraft pulp mill effluent.
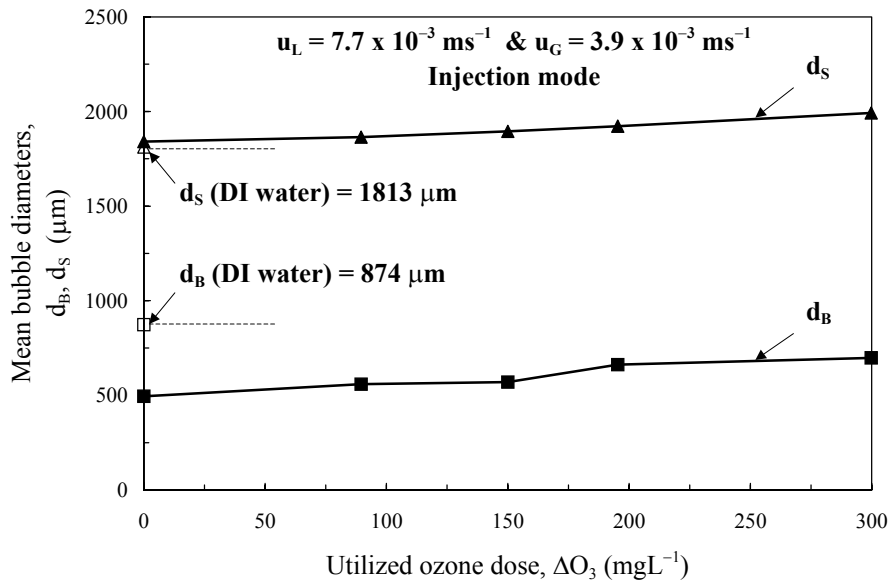

Figure 27.   Effects of ΔO_3 on d_B and d_S in Kraft pulp mill effluent.
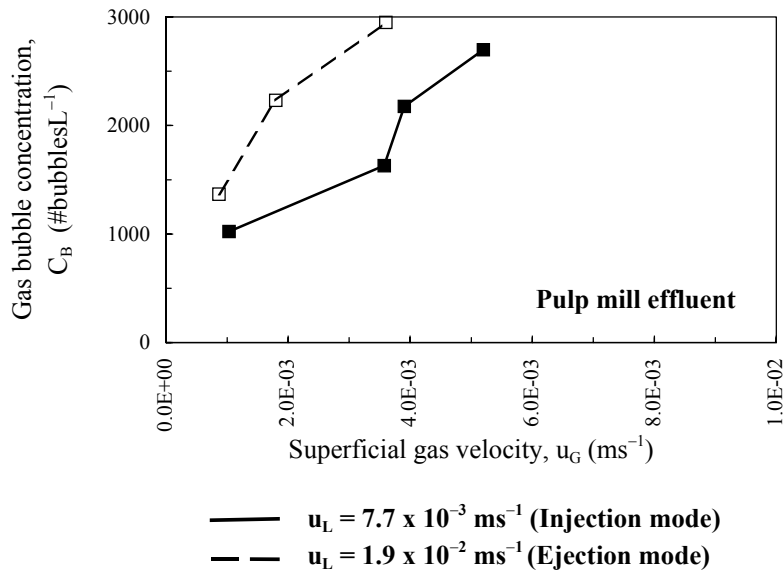
Figure 28.   Effects of u_G and u_L on C_B in raw Kraft pulp mill effluent.

The rate of increase in C_B per increase in u_G was doubled and the rate of increase in C_B per increase in u_L was almost identical in the raw Kraft pulp mill effluent compared to the deionized water. The effects of u_G and u_L on C_B are shown in Figure 28. Generally, based on the PDA measurement and visual observations, the gas-liquid flow during the aeration of Kraft pulp

mill effluent could be characterized as a homogeneous bubbly flow and the degree of homogeneity decreased as ΔO_3 increased. Under similar operating conditions, the higher homogeneity of the bubbly flow in the raw Kraft pulp mill effluent compared to the deionized water could be a result of the lower d_B and d_S, and the higher C_B observed in the raw Kraft pulp mill effluent. As a result of the lower d_B in the raw Kraft pulp mill effluent and under the same operating conditions, the bubble rise velocity (u) decreased by about 50 % compared to that in the deionized water. Therefore, lower d_B and d_S, higher C_B, and lower u caused the gas hold-up (ε_G) and the specific gas bubbles' interfacial area (a) to increase and they were about four times higher than those in the deionized water.

DETAILED REFERENCES

Detailed descriptions of the experimental methods and detailed results of the modeling of the ozonation treatment can be found in the following references:

Gamal El-Din, M. (2001). Theoretical analysis and experimental investigation of the performance of ozone bubble columns. Ph.D. Thesis, Department of Civil and Environmental Engineering, University of Alberta, Edmonton, Alberta, Canada.

Gamal El-Din, M., and Smith, D.W. 2001. Ozone mass transfer in water treatment: hydrodynamics and mass transfer modeling of ozone bubble columns. Wat. Sci. & Technol.: Wat. Suppl. 1(2): 123-130.

Smith, D.W., and M., Gamal El-Din 2001. Theoretical analysis and experimental verification of ozone mass transfer in bubble columns. Environ. Technol. (Accepted)

Gamal El-Din, M., and Smith, D.W. 2001. Development of transient backflow cell model (BFCM) for bubble columns. Ozone Sci. & Eng. 23(4): 313-326.

Gamal El-Din, M., and Smith, D.W. 2001. Designing ozone bubble columns: a spreadsheet approach to axial dispersion model. Ozone Sci. & Eng. (Accepted).

Gamal El-Din, M., and Smith, D.W. 2001. Maximizing the enhanced ozone oxidation of Kraft pulp mill effluents in an impinging-jet bubble column. Ozone Sci. & Eng. (Accepted).

Gamal El-Din, M., and Smith, D.W. 2001. Ozonation of Kraft pulp mill effluent: process dynamics. J. Environ. Eng. & Sci. (Accepted).

MANAGEMENT APPLICATIONS

This project involved the development of new design of ozone bubble column. This design has the potential to improve the ozonation treatment efficiencies, especially, when treating highly polluted industrial wastewaters such as pulp mill effluents. This new design of ozone bubble column can lead to significant reductions in the capital and operating costs compared to those encountered in conventional ozone bubble columns.

As a result of achieving higher treatment levels of pulp mill effluents, the ecological integrity of the boreal forest can be well maintained. Thus, this can lead to the preservation and improvement of the Canadian public and environmental health.

With the standards, that are used to regulate wastewater effluent discharges into the receiving environment, becoming more stringent, the need for effective treatment processes such as ozonation will become a necessity for many industries in order to comply with the stringent wastewater effluent quality standards.

CONCLUSIONS

Using the venturi injectors for sparging the ozone gas into the liquid phase in the impinging-jet contactor has led to a significant increase in the enhanced overall mass transfer coefficient (Ek_La) and the enhanced factor (E), compared to the other ozone contactors, over most of the studied range of the utilized ozone dose. As a result, the off-gas ozone concentrations that were produced from the impinging-jet contactor were substantially lower than those produced from the other contactors that were operated in a semibatch-flow mode.

The ozonation process induced higher reductions in the color and AOX concentrations compared to COD and TOC of the treated Kraft pulp mill effluents. The small ratio of the BOD_5/COD of the treated wastewater indicates the need for further treatment of this type of wastewater to increase its biodegradability, and consequently, to remove the increase in the BOD_5 of the wastewater as a result of applying further treatment. The reduction efficiencies of color, AOX, COD, and TOC indicated that the scale-up and reactor configuration have exhibited insignificant effects on the ozonation treatment levels achieved in the different types of the ozone contactors examined in this study. This suggests that a small scale-up factor was associated with the ozonation treatment of pulp mill effluents, especially at large scales, where there was virtually no effect on the ozonation induced reduction efficiencies of color, AOX, COD, and TOC. The treatment levels achieved in the impinging-jet and fine-bubble diffuser ozone contactors that were operated in a continuous-flow mode were compared and the two designs of ozone contactors were found to produce almost identical treatment levels except that the volume of the impinging-jet contactor was one seventh of that of the fine-diffuser contactor. Based on the above, it is evident that the operating costs of the ozonation process and the ozone off-gas destruction facilities will be greatly reduced when the impinging-jet ozone contactor is used for treating Kraft pulp mill wastewaters.

The 2-D laser and phase Doppler anemometry and the digital photographic measurement techniques provided great non-intrusive tools for characterization and better understanding of the gas bubbles in the impinging-jet bubble column. The digital photographic study provided valuable information on the shape and size of the gas bubbles as well as rough estimates of the bubble rise velocity that aided in optimizing the particle dynamics analyzer configuration and operational settings during the PDA study.

The PDA measurements provided rapid and accurate simultaneous measurements of the bubble size, bubble rise velocity, bubble size distribution, and gas-phase turbulence intensities in the impinging-jet bubble column that utilized two venturi injectors to create turbulent gas-liquid jets in the ambient fluid. These measurements were conducted in clean deionized water and Kraft pulp mill effluent that was ozonated using a wide range of utilized ozone doses. The intersecting of the gas-liquid jets caused an increase in the turbulence produced in the ambient fluid and as a result the count mean bubble diameter and the Sauter mean bubble diameter decreased and they were smaller than those obtained in conventional bubble columns. This has led to a significant increase in the specific bubble interfacial area compared to that in conventional bubble columns. The count mean bubble and Sauter mean bubble diameters were found to be dependent on the superficial gas and liquid velocities. The count and the Sauter mean bubble diameters were smaller in the raw Kraft pulp mill effluent compared to those in the deionized water. This has led to a significant increase in the gas bubbles' specific interfacial area and the gas hold-up compared to those in the deionized water. As the raw Kraft pulp mill effluent was ozonated and the amount of utilized ozone increased, the count mean and Sauter mean bubble diameters increased. The measurements of the gas hold-up and the specific gas bubbles' interfacial area obtained in the current study provided valuable information that will lead to a better understanding of the mass transfer process in clean environments such as deionized water as well as in highly reactive environments such as Kraft pulp mill effluents.

REFERENCES

Akita, K., and Yoshida, F. 1974. Bubble size, interfacial area, and liquid-phase coefficient in bubble columns. Ind. Eng. Chem., Proc. Des. Develop. 3: 84-91.

APHA-AWWA-WEF 1995. Standard Methods for the Examination of Water and Wastewater. 19th Ed. American Public Health Association, American Water Works Association, and Water Environment Federation, Washington, DC, USA.

Bauman, H.D., and Lutz, L.R. 1974. Ozonation of a Kraft mill effluent. Tappi J. 57(5): 116-119.

Canadian Pulp and Paper Association 1974. CPPA technical section, H5P Standard Method. CPPA.

DANTEC 1989. Particle dynamics analyzer: Users manual, DANTEC.

Deckwer, W.-D. 1992. Bubble column reactors, Cottrell V. (Trans.), Field R.W. (Ed.). John Wiley & Sons Ltd, Inc., Chichester, England.

Gamal El-Din, M., and Smith, D.W. 2001. Maximizing the enhanced ozone oxidation of Kraft pulp mill effluents in an impinging-jet bubble column. In Proceedings of the IOA/PAG Conference: Advances in Ozone Technology, Newport Beach, CA, USA.

Haberl, R., Urban, R. Gehringer, R., and Szinovata, R. 1991. Treatment of pulp-bleaching wastewaters by activated sludge, precipitation, ozonation, and irradiation. Wat. Sci. & Technol. 24: 229-239.

Heinzle, E., Geiger, F., Fahmy, M., and Kut, O.M. 1992. Integrated ozonation-biotreatment of pulp bleaching wastewaters containing chlorinated phenolic compounds. Biotechnol. Prog. 8(1): 67-77.

Jamialahmadi, M., and Müller-Steinhagen, H. 1992. Effect of superficial gas velocity on bubble size, terminal bubble rise velocity and gas hold-up in bubble columns. Develop. Chem. Eng. 1: 16-31.

Kaštánek, J., Zahradník, J., Kratochvíl, J., and Čermák, J. 1993. Chemical reactors for gas-liquid systems. Ellis Horwood, Chichester, England.

Metcalf and Eddy, Inc. 1991. Wastewater engineering: treatment, disposal and reuse. McGraw-Hill, Inc., NY, USA.

Mudde, R.F., Groen, J.S., and Van Den Akker, H.E.A. 1998. Application of LDA to bubbly flows. Nuc. Eng. & Des. 184: 329-338.

Mudde, R.F., Groen, J.S., and Van Den Akker, H.E.A. 1997. Liquid velocity field in a bubble column: LDA experiments. Chem. Eng. Sci. 52: 4217-4224.

Mohammed, A., and Smith, D.W. 1992. Effects of ozone on Kraft process pulp mill wastewater. Ozone Sci. & Eng. 14: 461-485.

Nebel, C., Gottschling, R.D., and O'Neil, H.J. 1974. Ozone decolorization of pulp and paper secondary wastewaters. In Proceedings of First International Symposium: Ozone for Water and Wastewater Treatments, Volume 1: 625-651.

Prat, V.M., Esplugas, S. 1989. Ozonation of bleaching water of the paper industry. Wat. Res. 23: 51-55.

Roustan, M., Wang, R.Y., and Wolbert, D. 1996. Modeling hydrodynamics and mass transfer parameters in a continuous ozone bubble column. Ozone Sci. & Eng. 18: 99-115.

Shawwa, A.R. (1998). Rational approach for dissolved air floatation contact zone modeling. Ph.D. Thesis, Department of Civil and Environmental Engineering, University of Alberta, Edmonton, Alberta, Canada.

Stanley, K.N., and Nikitopoulos, D.E. 1996. Bubble measurements in a gas-liquid jet. Chem. Eng. Comm. 143: 1-22.

Unno, H., and Inoue, I. 1980. Size reduction of bubbles by orifice mixer. Chem. Eng. Sci. 35: 1571-1579.

Voigt, J., and Schügerl, K. 1979. Absorption of oxygen in counter-current multistage bubble columns-I. Chem. Eng. Sci. 34: 1221-1229.

Yamashita, F., Mori, Y., and Fujita, S. 1978. Sizes and size distributions of bubbles in a bubble column-comparison between the two point electric probe method and the photographic method. J. Chem. Eng. Japan 12: 5-9.

Zhou, H., and Smith, D.W. 1997. Process parameter development for ozonation of Kraft pulp mill effluents. Wat. Sci. & Technol. 35(2-3): 251-259.

Zhou, H., and Smith, D.W. 2000a. Ozonation dynamics and its implication for off-gas ozone control in treating pulp mill wastewaters. Ozone Sci. & Eng. 22: 31-51.

Zhou, H., and Smith, D.W. 2000b. Ozone mass transfer in water and wastewater treatment: experimental observations using a 2D-Laser particle dynamics analyzer. Wat. Res. 34: 909-921.